FABRICATION OF ZINC OXIDE – BASED DYE SENSITIZED SOLAR CELLS USING BIOLOGICAL, MINERAL AND SYNTHETIC DYES

A THESIS PRESENTED TO THE
PHYSICS & MATERIALS SCIENCE
DEPARTMENT OF CHEMICAL, GEOLOGICAL AND PHYSICAL SCIENCES
COLLEGE OF PURE AND APPLIED SCIENCES
KWARA STATE UNIVERSITY, MALETE

BY

AMARACHUKWU NNEKA OSSAI
(16/27/MPH001)

IN PARTIAL FULFILLMENT OF THE REQUIREMENTS
FOR THE AWARD OF DEGREE OF
MASTER OF SCIENCE (M. Sc.)

AUGUST 2018

Certification

This dissertation titled ‘‘Fabrication of Zinc Oxide – Based Dye Sensitized Solar Cell using Biological, Mineral and Synthetic Dyes’’ by Amarachukwu Nneka Ossai has met all the requirements for the award of degree of Master of Science in Physics and Material Science of Kwara State University, Malete, and is approved for its contribution to knowledge.

PROF. A. O. AINA
MAJOR SUPERVISOR

DATE

DR. A. B. ALABI
CO-SUPERVISOR

DATE

PROF. A. O. AINA
HEAD OF DEPARTMENT

DATE

PROF. S. K. SUBAIR
DEAN OF POSTGRADUATE SCHOOL

DATE

Dedication

This project report is dedicated to my lovely husband, Mr. S. C. Ezike and my daughter and son, Chidalu Divinegrace and Chimeremeze Oluwadarasimi Praise, respectively.

Acknowledgements

To God almighty is all the glory for the completion of this project. My great gratitude goes to my lovely husband, Mr. S.C. Ezike for his support, encouragement and his invaluable understanding during the period of completing this work. I really cannot thank him enough. My gratitude goes to Prof. A. O. Aina, Head of Physics and Material Science Department, Kwara State University, Malete who is my major supervisor, for his guidance. Great appreciation goes to Dr. A.B. Alabi who is also my supervisor for his thorough guidance. He went through my work and saw to the success of this work from beginning to the end despite his tight schedule. In addition, my appreciation goes to the entire staff of Physics and Material Science Department, Kwara State University.

I would like to thank the staff of Engineering and Material Science Laboratory, Kwara State University, especially Mr. Biodun Rasheed for his assistance and guidance where necessary throughout my laboratory work and for providing the facilities to carry out the research.

My deepest gratitude goes to my family members for their prayer support and encouragement in the course of my studies.

Finally, I thank the staff of African University of Science and Technology (AUST) Abuja especially, Elechi Anthony, for providing the facilities to carry out some essential parts of this research.

Table of Contents

List of Figures

List of Plates

List of Tables

Abstract

Dye-Sensitized Solar Cell (DSSC) is a third generation solar cell, which comprises of semiconductor electrode, sensitizer, electrolyte and counter electrode. It utilizes the advantages of the large band gap of the semiconductor in cell, as a sensitizer. Natural dyes have become attractive as an alternative to expensive and rare organic sensitizers because of its low cost, non-toxic, high performance, price ratio, varieties of colors and environmentally friendly nature. On this note, fabrication of ZnO-based DSSCs using natural and synthetic dyes was investigated. On the course of arriving at the aim, the following objectives were carried out; (i) examination of morphology of ZnO thin films deposited by spin coating method, (ii) examination of absorption spectrum of dyes, (iii) obtaining I-V photoelectric characteristics of the fabricated cells and (iv) determining the efficiency of each fabricated cell. Commercial and biosynthesized ZnO powder were deposited using solution method (spin coating) and annealed at 500 ℃ for proper formation of the films. Extraction of the natural dyes (pawpaw leaf, beetroot, black cherry (plant dyes) and Yombo tumtum (mineral dye)) have been carried out and solution of synthetic dye from Eosin-Y also have been prepared. The absorption spectrums of the dyes were measured using UV-Vis Spectrophotometer and the dyes showed high absorption in the regions 500 – 750 nm, 450 – 600 nm, 450 – 600 nm, 400 – 700 nm and 450 – 550 nm for Pawpaw leaf, Beetroot, Black Cherry, Yombo Tum Tum and Eosin –Y, respectively. In addition, micro-structural and Structural analyses of ZnO films were carried out using Scanning Electron Microscope (SEM) and X-ray diffractometer. Then commercial ZnO coated substrates have been soaked in the different dye solutions and left for eighteen (18) hours. Graphite on FTO substrate served as counter electrodes and ZnO based-Dye Sensitized Solar cells fabricated. The performance, I-V curve and efficiency, of each cell have been characterized using solar simulator equipped with Keithley 2400 source meter. The characterization of the cells showed I-V characteristics with open circuit voltage (V_{oc}) 0.414V, short circuit current (I_{sc}) 0.01828 mA, Fill Factor (FF) 0.3594 and conversion efficiency (η) of 0.68% for pawpaw leaf dye-based cell. The V_{oc}, I_{sc}, FF, and η for black cherry dye-based cell were 0.4147V, 18.05 mA, 0.3756, 0.703%, respectively. The beetroot dye-based cell gave I-V parameters of 0.4147 V, 0.01103 mA, 0.3758 and 0.430% for V_{oc}, I_{sc}, FF, and η, respectively. In Yombotumtum dye-based cell, 0.391V, 15.41 mA, 0.3502 and 0.528 % were obtained for V_{oc}, I_{sc}, FF, and η, respectively. The Eosin-Y dye-based solar cell has I-V parameters of 0.4607 V, 22.9 mA, 0.440 and 1.161% corresponding to V_{oc}, I_{sc}, FF, and η, respectively. The optimized active material (black cherry) dye was used to fabricate solar cell based on biosynthesized ZnO solar cell and the characterization of the cell showed I-V characteristics with V_{oc} 0.3901V, I_{sc} 18.05 mA, FF of 0.3560 and conversion efficiency of 0.627%. This shows that natural dyes extracted from our daily used plants and mineral, which are environmental friendly, are suitable for use as light sensitizers in photovoltaic (PV) technology. Successful application of these materials in PV industries would reduce the cost of energy in the society.

CHAPTER ONE

1.0 Introduction

1.2 Background of study

Increase in energy demands and concerns over global warming have led to a greater focus on renewable energy sources in recent years. Burning of fossil fuels, natural gas, coal and oil releases harmful gases into the atmosphere. This causes pollution and is responsible for the green house effect where a greenhouse gas can absorb radiation in the infrared range creating the greenhouse effect considered the main cause of global warming. The increase of the amount of CO_2 produced in the combustion of fossil energy together with other greenhouse gasses; generate a reduction of the airflow with the consequent increase in insolation, which warms air in the atmosphere thus generating an overall increase of the temperature on the earth.

Therefore increasing the development and use of renewable energy technologies to sustain future growing energy consumption and reduce environmental pollution is getting more attractive. The sun is a primary source of energy for most life forms found on the earth as shown in figure 1.1.

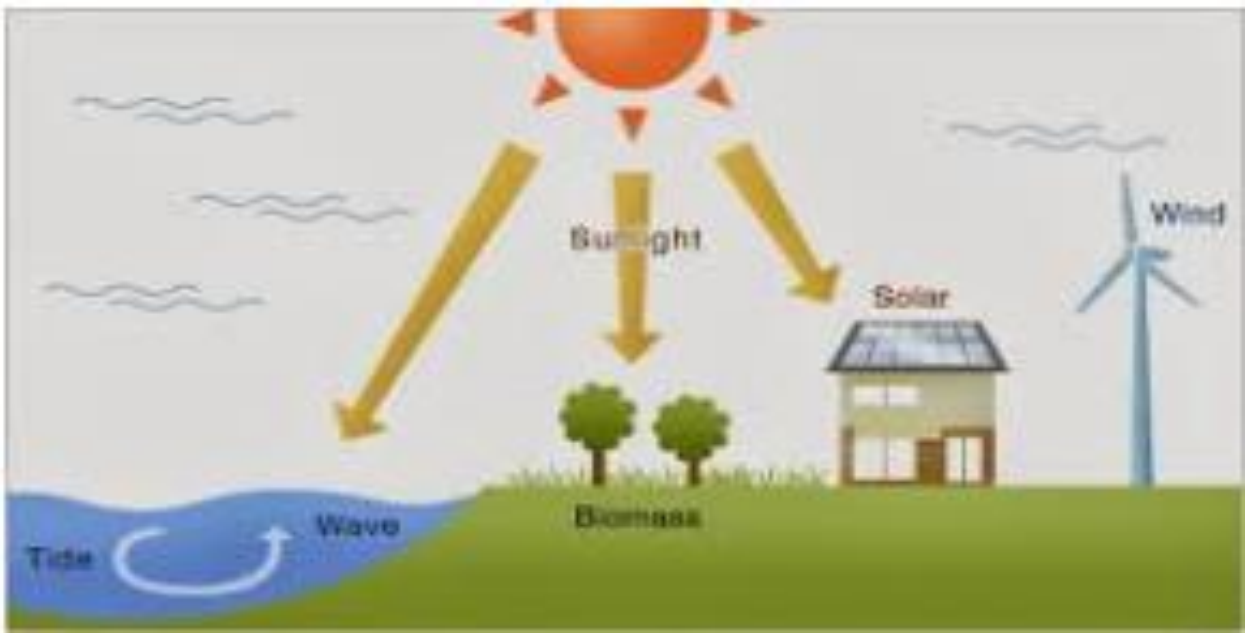

Figure 1.1: Sun as the dominant source of renewable energy (Partha, 2009).

Solar energy which has its source as the sun is considered as a feasible alternative because “more energy from sunlight strikes Earth in 1hour than all of the energy consumed by humans in an entire year” (Lewis, 2007). The world energy potential clearly indicates that most part of the world could potentially utilize the solar energy as the primary energy resources, especially for countries near the equator. Solar energy is a particular solution to the worlds energy need because it is inexhaustible, free and does not create greenhouse gases as it generates electricity (Pentland, 2010).

Solar cell is a light sensitive device that can harness solar energy and convert it into electrical energy as shown in figure 1.2.

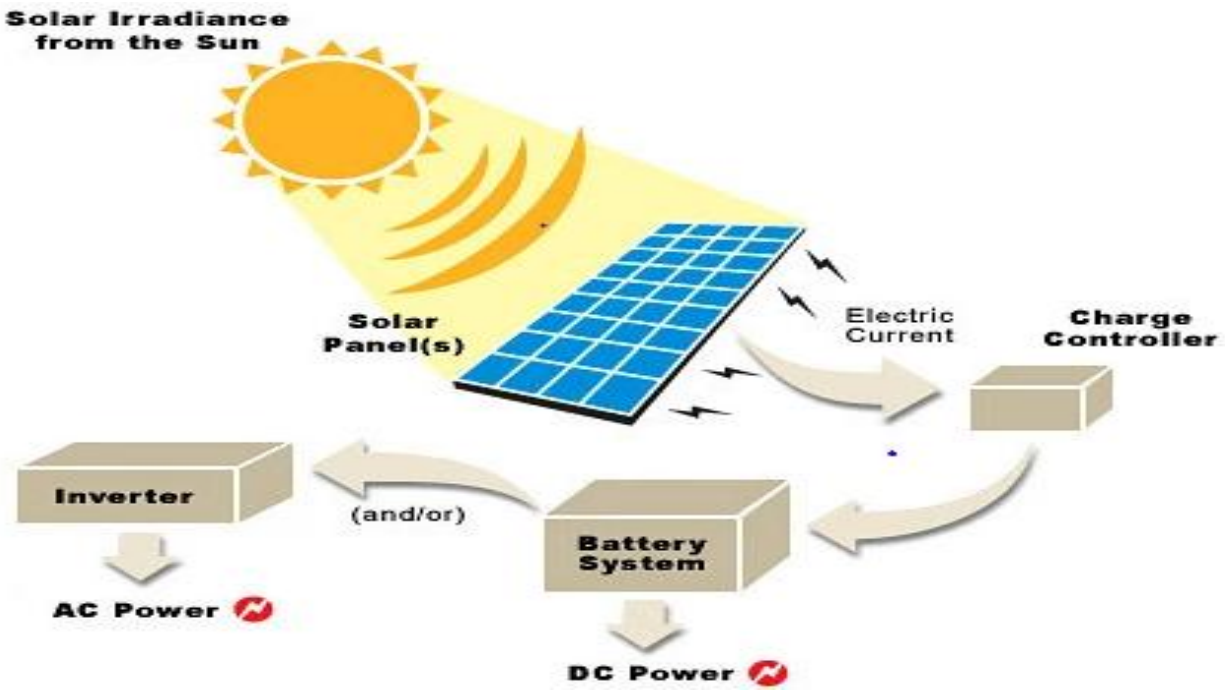

Figure 1.2: Conversion of solar energy to electrical energy (Partha, 2009)

The crystalline silicon based photovoltaic devices are the most widely used at present. The discovery of photovoltaic effect attributed to Edmond Becquerel in 1839 (Klar, 2005). He used metal halide salt solution with two electrodes immersed in it to describe the photovoltaic effect.

Photovoltaic technologies have a number of competitive advantages, such as zero noise, pollution free with little need for maintenance. The photovoltaic solar cells are in three major categories. Figure 1.3 shows the various generations of solar cells.

Figure 1.3: Solar cells generations reprinted (Noel *et al*., 2014)

(i) First generation of photovoltaic's (1970s): Solar cells made from crystalline silicon(C-Si) were the first used to supply energy to satellites. Silicon remains an attractive material, because it is among the most abundant elements on earth, mainly in the form of sand (SiO_2). It is a suitable semiconductor material for photovoltaic applications, with energy band gap of 1.1ev. It is of two types, we have monocrystalline (Mono C-Si) also called single crystals and polycrystalline (Poly-Si).

(ii) Second generation of photovoltaic's (1980s): The second generation technology uses layers of semiconductor materials in micrometers thickness (thin film) deposited on substrate such as glass, flexible plastics, or stainless steel. They require less semiconductor material to manufacture in order to absorb the same amount of sunlight. They are of three types; we have amorphous silicon (a-Si), Cadmium Telluride (Cd-Te), Copper-indium-selenide (CIS) and Copper- Indium-Gallium-diselenide (CIGS). Depending on the

technology, thin film module has reached efficiency between 7-15% (Greenet al, 2011).

(iii) Third generation of photovoltaic's (1990s): Third generation solar cells utilize the advantages of both the first and second-generation devices. Because of the low cost materials and easy fabrication, these technologies have become significant and attractive in the fast growing photovoltaic technology. The important means of producing high efficiency solar cells are reducing reflectance, trapping light in cell and increasing light absorption (Reshak *et al*., 2013).

Solar cell operation involves photon absorption by a semiconductor material. When photon is absorbed, the energy of photon transferred to valence electrons in crystal, which excites an electron to the conduction band, in which electrons can freely move. Figure (1.4) shows different band gap in conducting materials.

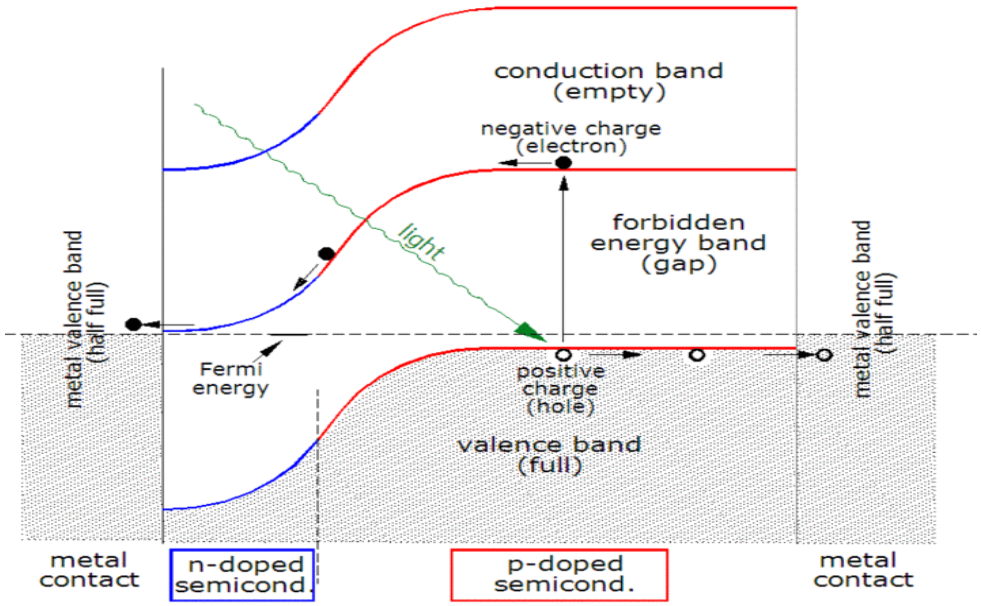

Figure 1.4: Band diagram of solar cell (Carlson, 1985).

Then the free electrons can move to one single direction because of the special composition of solar cells, which then generates current.

Figure (1.5) shows the complete structure of a common solar cell.

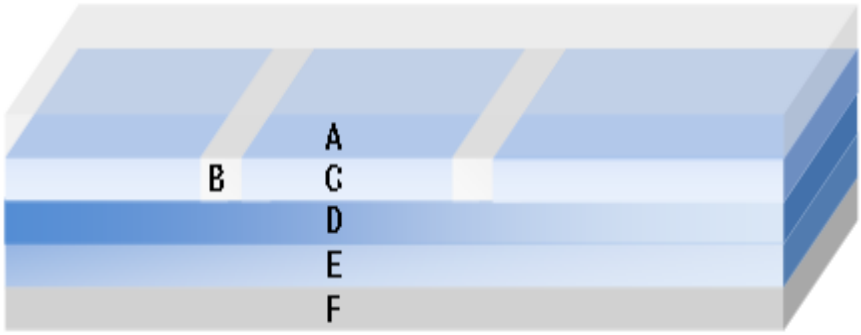

Figure 1.5: Structure of photovoltaic cell. (en.wikipedia.org)

The different parts in solar cell are the parts listed below:

- A: Encapsulate – An Encapsulate which is made of glass or other clear material which seals the cell from the external environment.

- B: Contact Grid- The contact grid is made of a good conductor, such as a metal, and it serves as a collector of electrons.

- C: The Anti-reflective Coating (AR Coating) - Through a combination of a favorable refractive index, and thickness, this layer serves to guide light into the solar cell. Without this layer, much of the light would simply bounce off the surface.

- D: N-Type Silicon - N-type silicon is created by doping (contaminating) the Si with compounds that contain one more valence electrons than Si does, such as with either Phosphorus or Arsenic. Since only four electrons are required to bond with the four adjacent silicon atoms, the fifth valence electron is available for conduction.

- E: P-Type Silicon- P-type silicon is created by doping with compounds containing one less valence electrons than Si does, such as with Boron. When silicon (four valence electrons) is doped with atoms that have one less valence electrons (three valence electrons), only three electrons are

available for bonding with four adjacent silicon atoms, therefore an incomplete bond (hole) exists which can attract an electron from a nearby atom. Filling one hole creates another hole in a different Si atom. This movement of holes is available for conduction.

- F: Back Contact - The back contact, made out of a metal, covers the entire back surface of the solar cell and acts as a conductor. (Specmat, 2009)

The current high cost of solar cells made from traditional inorganic semiconductors imposes a restriction on their mass usage. The silicon based photovoltaic technology is now being challenged by the emergence of third generation of cells, based, for example on nanocrystalline and conducting polymer films. These offer the prospective of very low cost fabrication and present attractive features that facilitate market entry. One of these is the Dye-Sensitized Solar cells.

Dye-Sensitized Solar Cells (DSSC) has emerged as an important cheap photovoltaic technology.

A Dye sensitized solar cell was invented by O'Regan and Gratzel in 1991. The DSSCs use earth abundant materials and have simple manufacturing processes, offering the potential to substantially reduce the photovoltaic electricity generation cost. DSSC is the third generation of solar cell, which comprises of a semiconductor electrode, sensitizer, electrolyte and counter electrode. At the heart of the device is a mesoporous film of semiconductor oxide nanoparticles, which coated with a monolayer of dye sensitive to the visible region of the solar spectrum. The DSSC utilizes the advantages of the large band gap semiconductor sensitized by light generated and excited electrons from the dye. The role of the dye is similar to the role of chlorophyll in plants. Compared to Si based solar cells, DSSCs are of low cost and ease of production. DSSC shows higher conversion efficiency than polycrystalline Si in diffuse light or cloudy

conditions (Khalil, 2011). Moreover, DSSC show higher conversion efficiency than polycrystalline Si in scattered light (Askari, 2016).

The table (1.1) below shows the comparatives between semiconductor solar cells and dye sensitized solar cells.

Table 1.1: Comparison between semiconductors based solar cell and DSSCs (Jasim, 201).

	Semiconductor Solar Cells	Dye-Sensitized Solar Cells
Transparency	Opaque	Transparent
Pro-environment (material & process)	Normal	Great
Power generation cost	High	Low
Power generation efficiency	High	Normal
Color	Limited	Various

The DSSCs is undergoing rapid development in an effort to obtain robust, efficient and cheap devices that are suitable for practical use.

The DSSC works by converting photon from solar energy to electrical energy, based on sensitization of wide band gap semiconductor (e.g TiO_2, ZnO and SnO_2), dyes (e.g N719, N3, organic dyes, natural dyes) and electrolyte (e.g I^-/I_3^- and Co^{2+}/Co^{3+} redox couple), (Bisqurt *et al.*, 2004) injected between the sensitizer and counter electrode (e.g platinuim and carbon materials) deposited on another conductive substrate (Ye *et al.*, 2014). In order to become an efficient solar cell, photo sensitizer, which is the organic dye layer, must have characteristics corresponding to the spectrum of available light. Different photo sensitizers will have different absorption of available light, thus a different efficiency and cost.

1.1.1 Key components of a Dye-Sensitized Solar Cell

The main components of the cell are substrate, a wide band gap semiconductor, the dye, electrolyte with a redox mediator and a counter electrode.

Substrate:

The front side illumination glass substrate acts as a window to the incident light and should be highly transparent in the visible –IR region. The substrate of the electrode serves as a collector for the current and therefore has to be a well transparent conductor. The substrate is also the mechanical support for the very thin semiconductor coating, which should strongly adhere to it.

On the other hand, the backside illumination through the counter electrode should have a reflecting photo electrode substrate to enhance light absorption by reflecting back the transmitted light into the dye. Indium-doped tin oxide (ITO) and fluorine-doped tin oxide (FTO) have been used in DSSCs. Due to poor thermal stability of the ITO layers, FTO glass is the preferred conducting substrate for the application in DSSCs. Sima *et al*., (2010) conducted a study based on FTO and ITO glass substrate sintered at 450ºC. They found that overall conversion efficiency of DSSC based on FTO and ITO are approximately 9.4% and 2.4% respectively. Thus FTO is strongly recommended for use in DSSC fabrication due to conductive properties and stable sheet resistance temperature.

Semiconductor oxide material

The central part of a DSSC device is made of a thick nano particle film (e.g TiO_2, ZnO, SnO_2 etc) that provides a large surface area for sufficient dye absorption and thus improves light harvesting efficiency and allow electronic conduction to take place (Suriati *et al*., 2015).

The advantages of nano sized semiconductor structure and particles include increased carrier lifetime arising from space quantization, enhanced redox

potentials of photo generated holes and electron arising from increased effective band gap.

TiO_2 has been the material of choice due to its high dielectric constant, which provides good electrostatic shielding of the injected electron from the oxidized dye molecule, thus preventing their recombination before reduction of the dye by the redox electrolyte (Monishkal, 2012).

Photosensitizers:

Due to the wide band gap of semiconductor oxide, it absorbs the photon up to 390nm. So that in order to harvest as much as possible of the solar spectrum reaching earth's surface, dye molecules which chemically bound to the semiconductor oxide surface acts as antennas. The performance of DSSC mainly depends on the molecular structure of the photosensitization. The ideal dye sensitizer for the photovoltaic should have the following characteristics:

- An intense absorption in the visible region and near IR regions of the solar spectra.
- Strong adsorption onto the semiconductor surface.
- Efficient electron injection into the conduction band of the semiconductor.
- The oxidized dye must have a more positive potential than the redox couple to prevent recombination of the injected electron with the oxidized dye.

Counter electrode:

The counter electrode is another critical component in DSSC where the mediator is reduced. The function of the counter electrode is to transfer the electrons arriving from the external circuit back to the redox electrolyte with the help of a catalyst such as graphite, platinum and carbon.

The counter electrode also has to carry the photocurrent over the width of each solar cell.

For efficient charge transfer, the counter electrode should exhibit a high catalytic activity and high electrical conductivity (Gao *et al*., 2012). It should also have a low charge transfer resistance and high exchange current density for the reduction of the oxidized form of the charge mediator.

The Electrolyte:

Electrolyte are used to regenerate the dye after electron injection into the conduction band of the semiconductor and also act as charge transport medium for the transfer of positive charge toward the counter electrodes (Mehmood *et al*., 2014).

Electrolyte can be of three types, liquid electrolyte, quasi solid electrolyte and solid electrolyte. The electrolyte used in DSSC mostly contains Iodide/triiodide redox ions, which mediate electron between the semiconductor oxide photo electrode and the counter electrode. The electrolyte in a DSSC works as a hole conducting medium. At the photoelectrode the oxidized dye, left behind by the electron injected to the conduction band of the TiO_2, is regenerated by the I^- present in the electrolyte, while at the counter electrode I_3^- is reduced to I^-. In other words, I_3^- is produced at the TiO_2 electrode, it diffuses into the electrolyte and at the end it is consumed at the counter electrode. In the same way, I^- is produced at the counter electrode, it diffuses into the electrolyte in the opposite direction with respect to I_3^- and finally it is consumed at the TiO_2 interface (Ferber *et. al*, 1998). Short circuit current density (Isc) and open circuit voltage (Voc) considerably depend on the electrolyte (Wu *et al*., 2008).

The electrolyte must have the following characteristics:

- High electrical conductivity

- Good interfacial contact with the nano crystalline semiconductor and counter electrode.
- No absorption of light in the visible region.
- The electrolyte should have long term chemical, thermal and electrochemical stability.
- The redox couple must be reversible at the counter electrode but should not react on the TiO_2 electrode.
- The redox couple must have a more negative electrochemical potential than the oxidized dye, so that reduction can take place.

1.1.2 The working principle of a Dye Sensitized solar cell

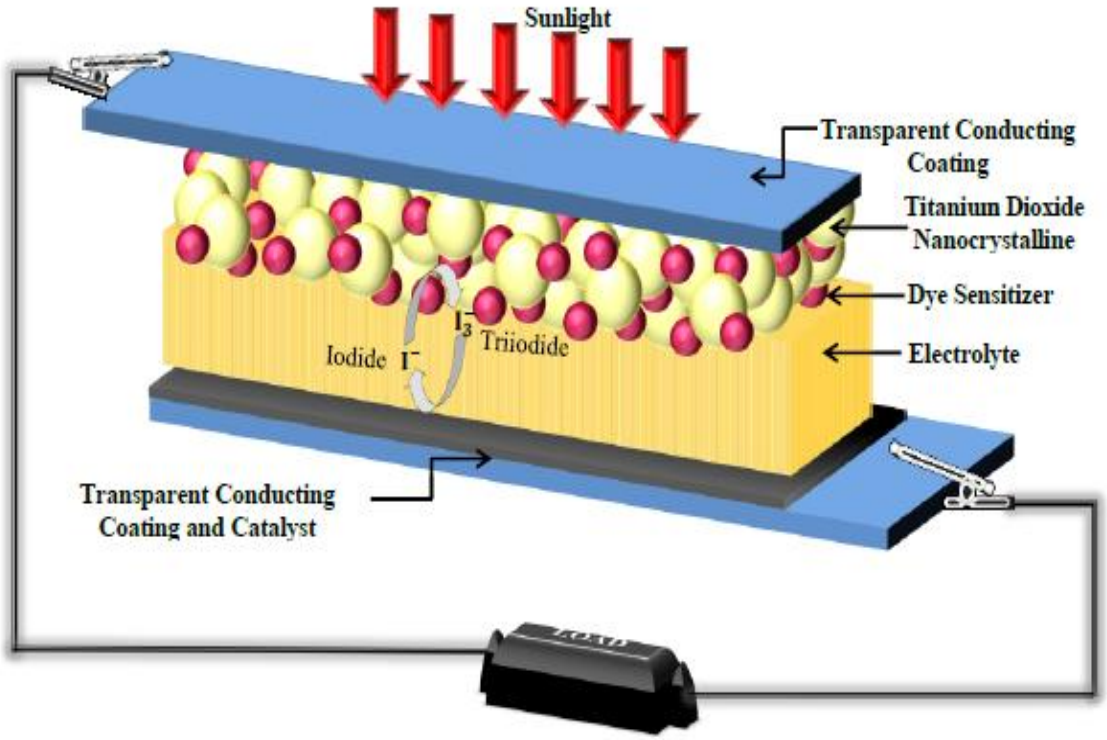

Figure 1.6: Principle of operation of DSSCs (Stathatos, 2010)

The DSSC differ from other solar cell types both by its basic construction and the physical processes behind its operation. Unlike the 1st and 2nd generation of PV devices based on solid semiconductor materials, the typical DSSC

configuration combines solid and liquid phases. The main difference to Si-based solar cells lies in the separation between charge generation (dye molecule) and charge-transport (TiO_2) and fact that charge separation occurs by means of kinetic irreversibility rather than by a built-in electrical field.

The working principle of DSSC is based on the photo generation of an electron by the dye, as in photosynthesis.

At the heart of a DSSC is a mesoporous layer composed of nm-sized particles of a wide-band semiconductor oxide, such as TiO_2, ZnO and SnO_2, that have been sintered together to produce electrical conductivity. Attached to the surface of the nano crystalline film is a mono layer of the charge transfer dye.

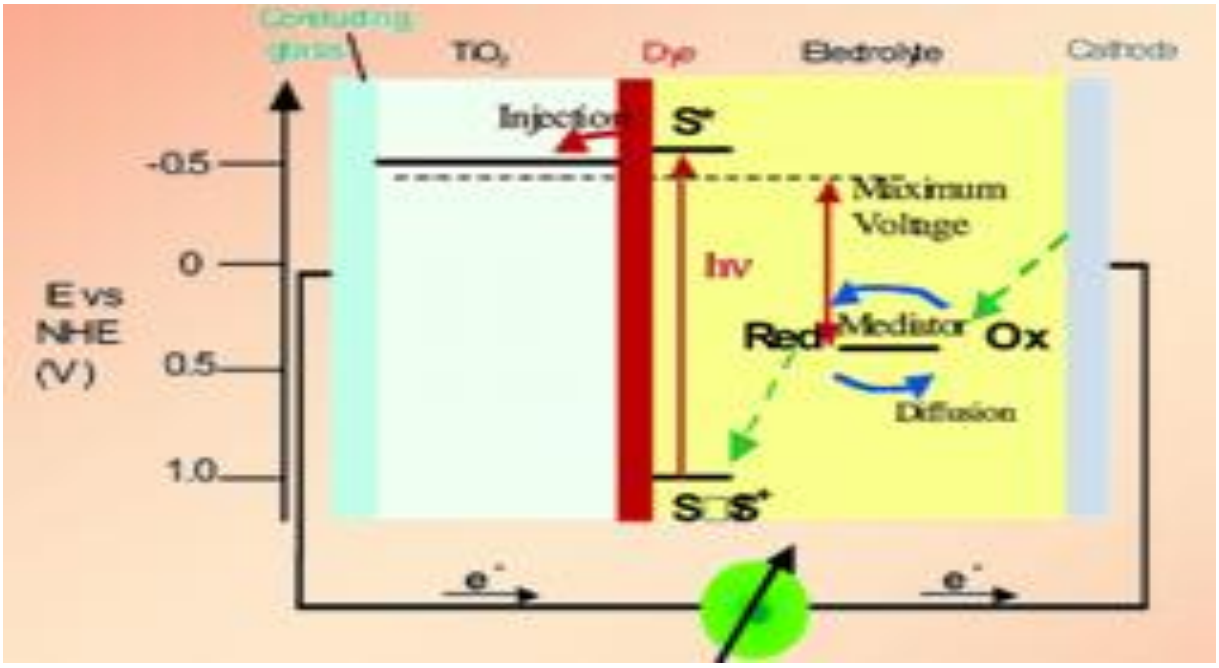

Figure 1.7: Energy level scheme of the DSSC (Graztel, 2003).

When a photon of light is absorbed by a dye molecule, an electron from the dye is excited from the highest occupied molecular orbital (HOMO) to the lowest unoccupied molecular orbital (LUMO) (Gregg, *et al*., 2001). This is followed by injection of the electron into the conduction band of the TiO_2. The injection of the electron into TiO_2 creates a hole in the dye generating the oxidized form of the dye.

After electron injection, the ground state of dye is subsequently restored by electron donation from the electrolyte reductant (Iodide), which in turn is regenerated by the reduction of the electrolyte oxidant at the counter electrode. The injected electron in the TiO_2 is transported to the counter electrode through the external circuit and recombines with triiodide to regenerate iodide. The internal circuit is completed by diffusion of the redox couple (iodide/Triiode) in the electrolyte. And the system continues so long as the sun shines on the cell.

Summary of the working principle:

- Photo excitation of the sensitizer.
- Electron injection into the conduction band of the semiconductor oxide film.
- Regeneration of dye molecule by redox system.
- Regeneration of the redox system at the counter electrode by electron passed through the load.

The operating cycle can be summarized in chemical reaction as (Mathews *et al*., 1996)

Anode

Photo excitation of the dye

$$S + hv \rightarrow S^* \qquad (1.1)$$

Electron injection in TiO_2

$$S^* \rightarrow S^+ + e^- (TiO_2) \qquad (1.2)$$

Regeneration of the dye.

$$2S^+ + 3I^- \rightarrow 2S + I^-_3 \qquad (1.3)$$

Cathode

Reduction of the redox.

$I^-_3 + 2e^- (Pt) \rightarrow 3I^-$ (1.4)

The main loss processes in a DSSC are:

- The relaxation of the excited electron to the ground state of the dye.
- The recombination of the injected electron with the oxidized dye.
- The loss of the injected electron in the conduction band to the triiodide electrolyte.

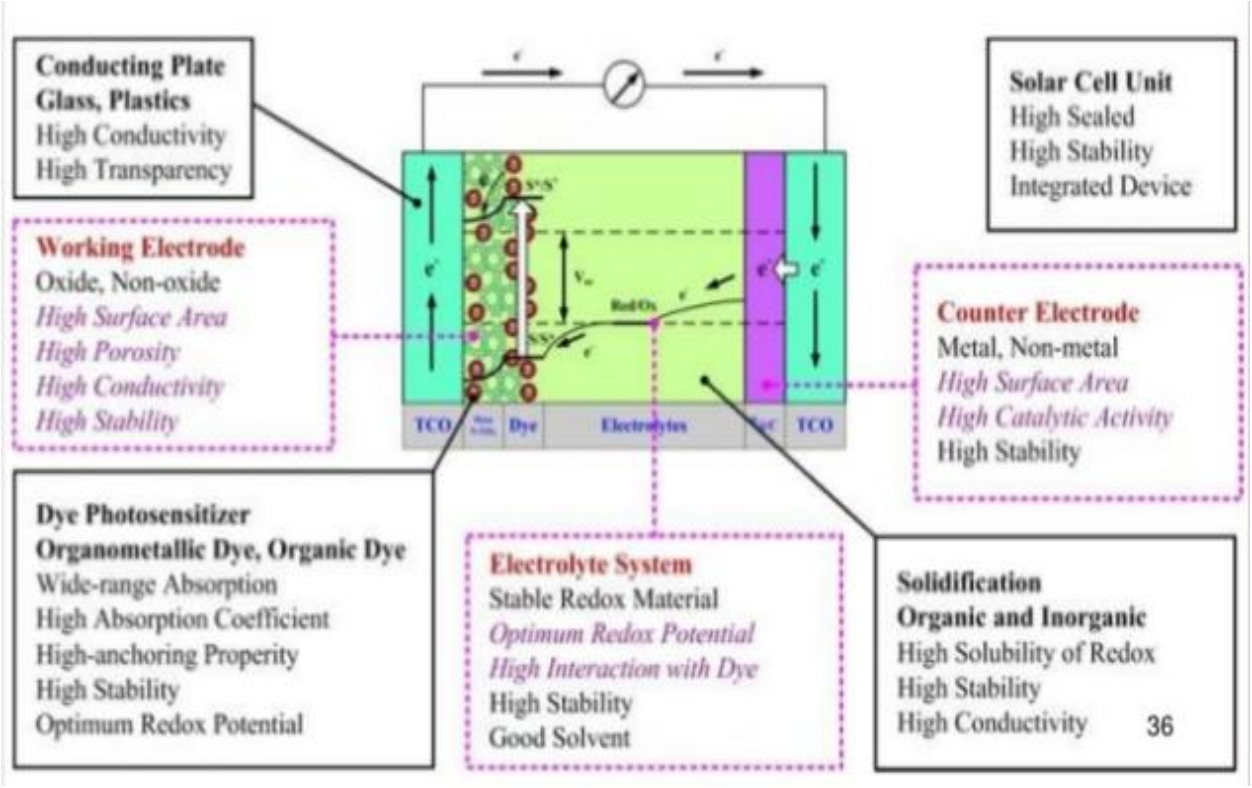

Figure 1.8: Summarized Properties of the components of the DSSC (en.wikipedia.org)

1.1.3 Charge separation

The charge separation in DSSCs is base on the electron transfer from the dye molecule to the TiO_2 and on the movement of the holes from the oxidized dye to the electrolyte. The electron transfer mechanism is strongly related to the electronic structure of the adsorbed dye molecule and the energy level matching

between the excited state of the sensitizer and the conduction band of the oxide semiconductor.

The main difference between the typical *p-n* junction cell and the one based on nanoparticle electrode/electrolyte interface is that the charge separation in silicon-based cell occurs at junction region where electric field is felt, but in a DSSC it is slightly different, because the small dimensions of the particles of the nanostructured electrode does not allow the generation of a field. The electrolyte surrounding all the nanoparticles decouples them and screens any electric field in a range of about a nanometer (Pichot and Gregg, 2000). Charge separation in DSSC occurs at interface between semiconductor oxide electrode and the dye. The most important mechanism for the separation of charges is however the relative position of the energetic levels: the excited level of the dye must be higher with respect to the conduction band of the oxide, and the HOMO level of the sensitizer must be below the redox potential of the electrolyte.

1.1.4 Charge transport

In a Dye-sensitized Solar Cell, the charge transport occurs at the electron transport in the nanostructured TiO_2 photoelectrode and to the hole transport in the electrolyte: both these mechanisms equally affect the overall performances of the cell. The semiconductor nanoparticle network works not only as a large surface area substrate for the dye molecules but also as a transport media for the electrons injected from the dye molecules [Hagfelt .A and Gratzel .M, 2000]. As mentioned above, the small size of the particles prevents the formation of a space charge layer and a built-in electric field inside the particles, and therefore the electrons cannot be drifted by an electric field. The collection of the electrons in the conduction band of the TiO_2 particles under illumination results in an electron concentration gradient in the electrode, and the electrons are transferred to the TCO back contact layer by diffusion. The movement of the electrons is characterized by a distribution of diffusion coefficients, related to

the hopping of the electrons via surface traps of different depths [Hagfelt and Gratzel, 2000]. These electron traps are localized energy states just below the conduction band edge of the semiconductor oxide and play a significant role in the electron transport. The diffusion coefficient of the electrons is strictly related with the position of the electron quasi-Fermi level under illumination. If the cell is exposed to a low illumination condition, only deep traps contribute to the electron transport, leading to a low diffusion coefficient. If the light intensity increases, the quasi-Fermi level rises and the number of traps contributing to the transport of electron increases. Allowing a higher diffusion coefficient and so a higher photocurrent.

1.2 Statement of the problem

Ruthenium based complex sensitizer which at present gives the best efficiency is very expensive and difficult to prepare (Furukaw *et al*., 2009). Thus an alternative organic dye such as natural dyes is suggested with similar characteristics and high absorption coefficients (Hagberg *et al*., 2008).

1.3 Significant of the study

Ruthenium based complex sensitizer, which at present gives the best efficiency is very expensive and difficult to prepare. The natural and mineral dyes are cheap, non-toxic, high performance price ratio, variety of colors and environmentally friendly in nature. The mineral dye (*Yombo tumtum*) used in this study does not degrade easily and might improve the life span of the cell. This makes DSSCs attractive as a replacement for existing technologies.

1.4 Aim

The purpose of this study is to fabricate ZnO-based dye-sensitized solar cells using biological, mineral and synthetic dyes.

1.5 Objectives

The objectives are to;

i. analyze the absorption spectrum of the dyes (pawpaw leaves, beetroot, black cherry, yombo tumtum and Eosin-Y),
ii. examine the properties of the zinc oxide thin film deposited using solution method,
iii. obtain the I-V photoelectric characterization of the fabricated cells and
iv. deduce the efficiencies of each cell fabricated.

1.6 Scope of the study

The study focuses on the fabrication of ZnO-based dye-sensitized solar cells using natural dyes extracted from black cherry, beetroot, and pawpaw leaf, mineral dye from yombo tumtum and synthetic dye from Eosin-Y. These dyes were subjected to UV-Visible spectrophotometer to measure the absorption spectrum of each of them. The zinc oxide thin film deposited using spin coating machine undergoes scanning electron microscope (SEM) to view the surface morphology.

Furthermore, solar simulator was used to determine the photoelectrochemical parameters of the fabricated cells.

This dissertation is divided into five chapters; the first chapter gives the introduction to the study by describing the background and purpose of the study as well as the short description of the

operating principle of the Dye-Sensitized solar cell. Chapter two introduces the literature review of dye-sensitized solar cell. Chapter three describes the materials of the DSSCs and the experimental procedure of the present study. Chapter four presents the results from the experimental part of the work, and finally, chapter five presents the conclusion and recommendation for further research.

CHAPTER TWO

2.0 Literature Review

2.1 The Dye-sensitized Solar Cell

In the past years, almost all the research effort focuses on the modification of each of the components of Dye-sensitized solar cells for practical application. Areas of interest have been, the construction of nanostructured semiconductor photoanodes with effective architecture for high dye loading and fast electron transport, the exploitation of versatile sensitizers with strong visible light harvesting ability, the utilization of the redox electrolyte with useful compositions for efficient hole transport, the optimization of the counter electrode as well as the development of other equivalent alternatives at lower costs.

The major challenge in the fabrication and commercialization of DSSC is the low conversion efficiency and stability of the cell. The degradation of the cell based on dye sensitization, undesirable electrolyte properties and poor contact with electrodes are the main causes of the poor performance of DSSCs (Suriati Suhaimi *et al*., 2015).

2.1.1 Photosensitizers

Several number of sensitizers that have been developed in the fabrication of DSSC includes, ruthernium dyes, porphyrin and phthalocyanines dyes, metal free organic dyes, natural dyes.

They have different degradation mechanism and their degradation is mainly caused by elevated temperature, attachment of water or oxygen from the air and UV irradiation that oxidizes the dye molecules. There may be a back-reaction that takes place between the conduction band electrons from the excited sensitizers and oxidized dye molecules themselves, or with the oxidized electrolyte species. (Mohammed *et al*., 2015).

2.1.2 Ruthenium – based dyes

Ruthenium-based complexes are the most common used sensitizers for DSSCs (e.g N719, N3, N749). A number of new ruthenium dyes have been developed to address the problem of dye degradation in the presence of water and at elevated temperature.

The finest photovoltaic performance in terms of both conversion yield and long term stability has so far been achieved with polypyridul complexes developed by the Gratzel group (N3, N719 and black dyes).

Ru(11) is the most efficient dye due to its numerous advantageous features, such as good absorption, long excited state lifetime, and highly efficient metal to ligand charge transfer (Suraiti *et al*., 2015).

The degradation mechanisms of Ru-dyes (e.g N719, N3, N749) have been studied by a number of researchers using UV-Vis, IR and Raman spectroscopy (Likodimos *et al*., 2009; Greijer *et al*., 2003). From their experimental results, it appears that the weakest parts of Ru-dyes are the Thiocyanate donor ligands (SCN^-) (Greijer *et al*., 2003). These studies indicate that the thiocyanate ligands tend to be lost when the temperature is equal to or above 135 ℃ and are prone to exchange with H_2O/OH^- and I_3^- in the air or in the electrolyte. Therefore, to prevent the degradation of Ru-dyes in DSSCs, the device needs sealing to exclude O_2 and H_2O or the Ru-dyes replaced with dyes that have more tolerance towards O_2 and H_2O.

2.1.3 Porphyrin dyes

They have intense absorption range from ultraviolet to near infrared light, excellent molecular stability and appropriate energy levels with versatile structures. Another strategy to obtain a broad optical absorption extending through the visible and near IR region is to use a combination of two dyes which complement each other in their spectral features. After various attempts, a recorded power conversion efficient of 12.3% for liquid electrolyte DSSC was

obtain in 2011 by using a zinc porphyrin dye YD2 -0-C8 co- sensitized with another organic dye (Y123), and $CO^{11}/^{111}$ based redox electrolyte at AM 1.5 global full sun (Yella *et al*., 2011) .

Porphyrin-sensitized DSSC with the YD-2 dye attained a PCE of 11% in 2010, which was further increased to 11.9% by using another porphyrin dye (YD-2-0-C8) in 2011.

2.1.4 Natural dyes

Natural dyes are viable alternatives to expensive organic based DSSCs (Arjunan and Senthil, 2012). Natural dyes include plant dyes, animals and mineral dyes. Plant dyes can be obtained from roots, flowers, leaves, fruits and back of plants such as wood and indigo. Some animal sources of dyes include insects such as cochineal, found on cacti in Mexico, Lac found in India and Iran and Kermes found on oak tree near the Mediterranean. Mineral dyes come from ocher (yellow, brown, red), limestone or lime (white), manganese (black), cinnabar and lead oxide (red), azurite and lapis lazuli (blue) and malachite (green) (Wayne, 1994). Different parts of the plant, including the flower petals, fruits, leaves, stems and roots, typically have different pigments. The advantages of natural dyes are their low cost, easy extraction, non-toxicity and environment friendly nature and being fully biodegradable (Dai and Rabani, 2002). Natural pigments, including chlorophyll, carotenoids, anthocyanin, nasunin and crocetin are freely available in plant leaves, flowers and fruits and potential to be used as sensitizers (Narayan, 2012). Natural dyes as light harvesting elements in DSSCs can contribute to a sustainable solution for the future energy production (Hug *et al*., 2014). The achievement of wide-bandgap semiconductor sensitization using natural pigments is typically attributed to Anthocyanin. Mamidi *et al*., (2012) studied some of these dyes including dried palash flowers, dried Hibiscus flowers, beet, pomegranate, red wine, mechandi, turmeric. Out of all these, dye made of dried hibiscus leaves have given best result. The Anacardium

occedentale sensitized dye solar cell exhibited a very high fill factor which suggests efficient packing at the TiO_2 electrolyte interface (Oviri and Ekpunobi, 2012).

2.1.5: Anthocyanins

The achievement of wide band gap semiconductor sensitization using natural pigments is typically attributed to anthocyanins. The anthocyanins consistitute a major flavonoid group that is responsible for cyanic colors ranging from salmon pink through red and violet to dark blue of most flowers, fruits and leaves of angiosperms (Narayan, 2012). Sometimes they are usually in solution within the vacuole, although they may sometimes be located in spherical vesicles called antocyanoplast. They are a group of naturally occurring phenolic compounds responsible for the color of many flowers, fruits (particularly berries) and vegetables. Anthocyanins molecule possesses carboxyl and hydroxyl groups and it occurs in fruits, leaves and flowers. Anthocyanins are often used in organic solar cells due to their ability to absorb light and convert it into electrons. The absorption maximum of the antocyanine dye solution extracted from blackberries is 545nm (Michal *et al.*, 2011). The absorption of the linked dye to TiO2 showed a slight shift to the wavelengths with a value of 540nm. The sensitizers in natural dyes are linked to the anthocyanins, carroten, tannin and chlorophyll present in the plants (Woncharee *et al*., 2007). These constituent molecules in form of carbonyl and hydroxyl group occurs naturally in fruits, leaves and flowers and are responsible for the exhibition of the types of color observed in the visible red-to-blue spectrum.

Natural dyes as photosensitizers are very attractive because they are of low cost, non-toxic abundant in supply and sustainable.

2.2 The Redox Mediators

Redox mediators and electrolyte systems have been explored, including Iodide/triode in either solid polymer, gel, ionic liquid, or plastic crystal systems, solid inorganic materials, CO^{11}/CO^{111} and $Sec^{-1}/(SecN)_3$ redox couples. Researchers achieved reduced efficiency so far for such cells. The cells that displayed the highest efficiency used an Iodide/triode redox electrolyte solution (Neil, 2009).

Important factor associated with the stability of DSSCs is the degradation of electrolyte components because of inadequate device sealing.

This degradation probably related to decrease of the triiodide concentration, reaction of electrolyte components with sealing materials and evaporation of the electrolyte solvents.

Because of the decrease of triiodide concentration, the diffusion resistance of Iodide/triiodide redox couples increased and thus led to an increase of the total series resistance of the cell. Because of this the fill factor and I_{sc} decreased (Kato *et al*. 2009).

A disadvantage of the liquid electrolyte is that it may limit device stability because the liquid may evaporate when the cell is imperfectly sealed. Penetration of water or oxygen molecules and their reaction with the electrolyte may also worsen cell performance.

Electrolyte solution contains volatile organic solvent which must be carefully sealed as they are hazardous to human health and the environment. In general, there are certain criterias, which materials should fulfill to acts as an electrolyte such as, it should have high conductivity, highly stable, chemically inert and does cause desorption of the dye from the photoanode (Chiba *et al*., 2006).

Presently, a non-volatile redox mediator is desired to avoid leakage and instability problems inherent to the liquid system. Ionic liquids are a promising electrolyte alternative providing advantages such as non-volatility, high thermal and chemical stability and excellent ionic conductivity. However, DSSCs based

on highly viscous ionic liquids often result in mass transport limitations retaining the PV performance in particular at high light intensities (Klar, 2005).

Replacing the liquid electrolyte with a solid has been a major ongoing field of research. Recent experiment using solidified melted salts have shown some promise, but currently suffer from higher degradation during continued operation, and are not flexible (Arjunan and Senthil, 2013).

The interaction of electrolyte additives, electrolyte cations and H_2O at the TiO_2/dye/electrolyte interface plays a significant role in the photovoltaic performance of the DSSCs, as well as in the stability of the cells, because changes of electrochemistry at the interface affect the kinetic performance of the solar cells (Ye *et al*., 2014).

One alternative which offers itself to confront the sealing problem is the replacement of the redox electrolyte by a solid P-type semiconductor interpenetrating the nanocrystalline TiO_2 structure which would permit the charge neutralization of the dye molecules after electron injection by its hole transport properties (Gratzel, 2003).

2.3 Photoelectrode

The stable electron collection efficiency is vitally important for prolonged operation of DSSCs and it is dependent on the electrical contact between TiO_2 nanoparticle and on the connecting substrate (Bisquert *et al*., 2004). The TiO_2 may lose contact with each other and with the substrate overtime, thereby increasing the transport resistance under thermal or mechanical stress.

Alternative method of improving the connection has been investigated, and compression of the TiO_2 particles after the deposition is the most successful technique to date (Weerasinghe *et al*., 2011).

To enhance the light harvesting properties of TiO_2 from UV region to the visible region, doping it with oxides of earth abundant metals and friendly metals is another option (Atishay *et al.* 2017). (Lu *et al.*, 2010) studied the effect of

Niobium (Nb) doped anatese TiO_2 on the performance of DSSC. It was found that doping of (Nb) has a positive effect on the photocurrent and this positive effect is due to the enhanced electron injection and increased charge transfer kinetics. The important means of producing high efficiency solar cells are reducing reflectance, trapping light in the cell and increasing light absorption. (Reshak *et al*., 2013). H. Chang et al. used TiO_2-CNT (carbon nanotube) composite material as photoelectrode for enhancing the efficiency of DSSC.

ZnO is an alternative semiconductor oxide material due to its wide band gap similar to TiO_2, and its ability to be synthesized simply with different nanostructures. The advantages of ZnO over TiO_2 include the following (Chergui *et al*., 2011):

- A direct band gap of approximately 3.37eV
- A higher excitation binding energy (60meV) compared with TiO_2 (4meV) and
- Higher electron mobility ($200cm^3V^{-1}S^{-1}$) compared with TiO_2 ($30cm^3V^{-1}S^{-1}$) and carrier lifetime.

The grain size of ZnO is overly large, and its effective surface area is insufficient; hence, the efficiency of ZnO is low. Therefore; the key to improve the performance of ZnO-based Dye sensitized solar cell is the preparation of a nanoporous ZnO film.

Mahmood et al. synthesized boron-doped ZnO film as photo anode for the fabrication of DSSC. They reported the high conversion efficiency of about 7.2% with the use of electrons towards the electrodes and also function as light scattering centers. The transport rate of electron is faster in ZnO compared to TiO_2, whereas the recombination rate on the other hand is also higher (Kumar *et al*., 2014).

To obtain effective photoanodes, a variety of film preparation techniques, such as sol-gel (Bahramain, 2013) electrochemical anodization (Mir *et al*., 2012), Spray pyrolysis (Huo *et al*., 2013) and atomic layer deposition (Son *et al*.,

2013) have been developed and applied for craft semiconductor photoanodes. Post treatment of TiO_2 film with $TiCl_4$ is an efficient method to improve the efficiency of TiO_2 nanaoparticle based DSSC. It yielded an efficiency of 7.83% (Hyuk *et al*., 2014).

2.4 The Counter Electrode

Platinum is the most efficient and commonly used catalyst material and can be applied onto the flexible substrate by various low temperature methods, such as sputtering, vapor, chemical or electrochemical deposition (Kim *et al*., 2006; Ito *et al*., 2006). In the chemical and electrochemical methods, platinum is reduced on the substrate surface from its salt solution. The reduced platinum particles are always quite weak in terms of adhesion to the substrate. Weakly adhered platinum particles are likely to diffuse into the electrolyte or onto the working electrode and act like recombination centers (Toivola *et al*., 2009). They reduce the photovoltaic performance of DSSCs during prolonged thermal or light soaking stress.

A number of alternate materials such as conductive polymers (e.g. PEDOT) (Pringle *et al*., 2010), carbon-based materials (Veerappan *et al*., 2012) and electrochemically deposited CoS (Lin and Liao, 2012) have been successfully applied to replace the expensive platinum as counter electrode materials for flexible DSSCs.

In summary, stability is regarded as the main limiting factor preventing the DSSCs from commercialization. In other to improve the stability in DSSCs, these approaches mentioned below have been suggested;

- Applying UV irradiation filters also known as polyster films.
- Adding MgI_2 or CaI_2 to the electrolyte to enhance the electrolyte tolerance towards UV irradiation.

- Coating a thin layer (1-3nm) of wide band gap MgO or Al_2O_3 on the TiO_2 to avoid the decomposition of the cell components in contact with TiO_2 surface (Hinsch *et al*., 2001; Lin *et al*., 2009).

2.5 Photoelectrochemical Parameters

A photovoltaic cell is a device that converts the incident sunlight to electrical energy, exploiting the photoelectric effect. The generation of the electrical power under illumination is achieved by the capability of the photovoltaic device to produce voltage over an external load and current through the load at the same time. Figure (2.1) shows the typical current-voltage (I-V) characteristic of a solar cell. The current-voltage (I-V) characteristics of a solar cell under illumination are used to determine the power conversion efficiency (η) of the cell. From the I-V curve, the short circuit current density (Jsc) is determined at th V = 0 intercept, while the open circuit voltage (V_{oc}) is found at the $J_{sc} = 0$.

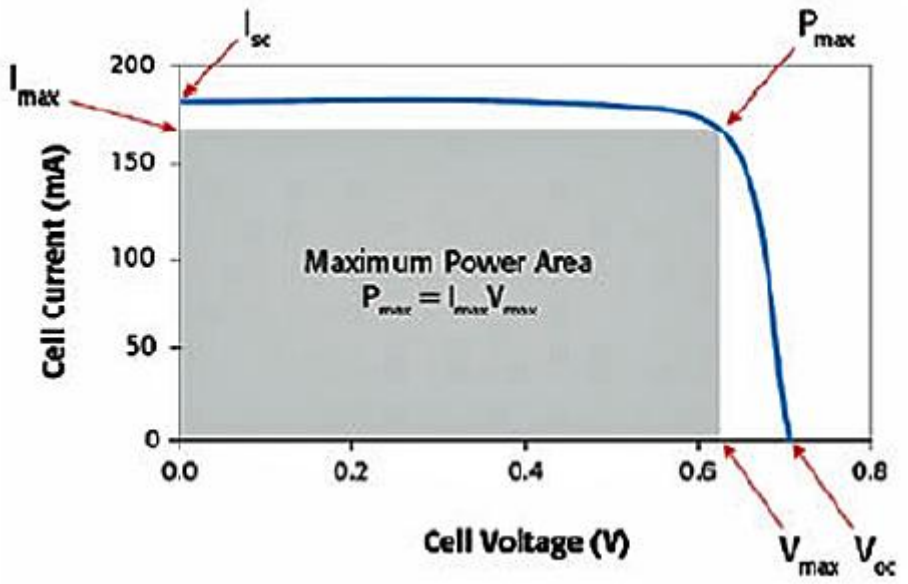

Figure 2.1: Typical I-V characteristic of solar cell
(http://www.keithley.com/solar_cell)

2.5.1 Incident photon to current conversion efficiency (IPCE)

The spectral response of the dye sensitized solar cell depends on the absorption properties of the dye. The incident photon to current conversion efficiency also known as external quantum efficiency (EQE) is one of the key parameters of quantitative characterization of the solar cell performance for the fact that IPCE shows the spectral response of solar cells to various incident wavelengths. It measures how efficiently the incident light of a specific wavelength is converted into electron/hole pairs, by measuring the ratio between the number of electrons generated by the solar cell and collected at the external circuit and the number of photons of a giving wavelength of light shining on the solar cell.(Saito *et al*., 2002).

The equation of IPCE stated in equation (2.1).

$$\text{IPCE} = \frac{1240.\text{Jsc}}{\lambda.\text{Pin}} \qquad (2.1)$$

where J_{sc} is the short circuit photocurrent density (mA/cm^2), λ is the wavelength (nm), P_{in} is incident power (mW/cm^2).

2.5.2 Open circuit voltage (V_{oc})

The open circuit voltage V_{oc} is the maximum voltage generated by the solar device when no current flows and defined as the different between the potential of the conduction of the TiO_2 and the redox potential of the electrolyte. V_{oc} is measured when the circuit is open or external load is connected. Under this condition, there is no external current flows between the two terminals i.e. I = 0 and $V = V_{oc}$. It depends on both Fermi level of the semiconductor and level of dark current. The theoretical maximum of the V_{oc} of the cell is determined by the redox potential of the electrolyte.

2.5.3 Short circuit photocurrent density (J_{sc})

The short circuit (J_{sc}) represents the maximum current when the electrodes are short-circuited. Short circuit is the photocurrent per unit area (mA/cm^2) when an

illuminated cell is short- circuited where the external output voltage is zero. It depends on several factors such as the light intensity, light absorption, injection efficiency of charge transport in the TiO_2 film to the counter electrode. Theoretical values of J_{sc} can be calculated from integral sum of incident photon to current conversion efficiency (IPCE) as in equation (2.2).

$$J_{sc} = \int_0^{\infty} IPCE(\lambda).Isun(\lambda)d\lambda \quad (2.2)$$

While maximum power point, P_{max}, is the point in which the product of the current and the voltage is maxima.

2.5.4 Fill factor (FF)

Another important parameter obtainable from the I-V characteristics is the fill factor FF, which is a measure of the cell quality and defined as the squareness of the I-V curve. Equation (2.3) is used to calculate FF.

$$FF = \frac{I_{max} \times V_{max}}{I_{sc} \times V_{oc}} \quad (2.3)$$

2.5.5 Solar energy to electricity conversion efficiency (η)

The overall solar energy to electric power conversion efficiency (η), the key parameter of the device, measures how much power converted by the cell in comparison to the amount of absorbed light that reach the device.

Equation (2.4) is used to calculate the solar energy-to-electricity conversion efficiency (η).

$$\eta = \frac{I_{sc} \times V_{oc} \times FF}{P_{in}} \quad (2.4)$$

Where P_{in} is the power of incident light and measure in $mWcm^{-2}$ using a solarimeter and I_{sc} measured in $mAcm^{-2}$ (Wenhan *et al*., 2006).

2.6 Spectroscopic Analysis

Ultraviolet and visible (UV-VIS) absorption spectroscopy is the measurement of the attenuation of a beam of light after it passes through a sample or after reflection from a sample surface. Ultraviolet-visible near-infrared (UV-VIS-

NIR) spectroscopy is useful to characterize the absorption, transmission, and reflectivity of a variety of technologically important materials, such as pigments, coatings, windows, and filters. In color pigment, what human eye perceives as the color of a dye is the combination of the wavelength not absorbed but reflected. The light absorbed by the chromophore of a dye is of the complementary color of the apparent color of the dye. Chlorophyll absorbs mostly blue and red, and the complementary color it reflects is green, while anthocyanins absorb blue and green, giving us perception of a red or violet color (Klar, 2005).

Table (2.1) below shows the relationship between the absorbed and complementary colors in the UV and visible region.

Table 2.1: Relationship between absorbed and complementary color (perceived) in the visible spectrum (Bailey et al., 2002).

Absorbed wavelengths/nm	Absorbed color	Complementary color
380-420	Violet	Green-yellow
420-440	Violet-blue	Yellow
440-470	Blue	Orange
470-500	Blue-Green	Red
500-520	Green	Purple
520-550	Yellow-green	Violet
550-580	Yellow	Violet-blue
580-620	Orange	Blue
620-680	Red	Blue-green
680-780	Purple	Green

Spectrophotometer is an instrument used in measuring the intensity as a function of the color or wavelength of the light (Chang *et al*., 2010). Other important features of spectrophotometers used in the UV and visible regions of the spectrum, as well as into the near-infrared region. There are two major

classes of spectrophotometer; single beam and double beam. A double beam spectrophotometer measures the ratio of the light intensity on two different light paths and a single beam spectrophotometer measures the absolute light intensity. The basic parts of the spectrophotometer are light source, light filter, monochromator, sample holder(s), recorder and detector as shown in figure (2.2).

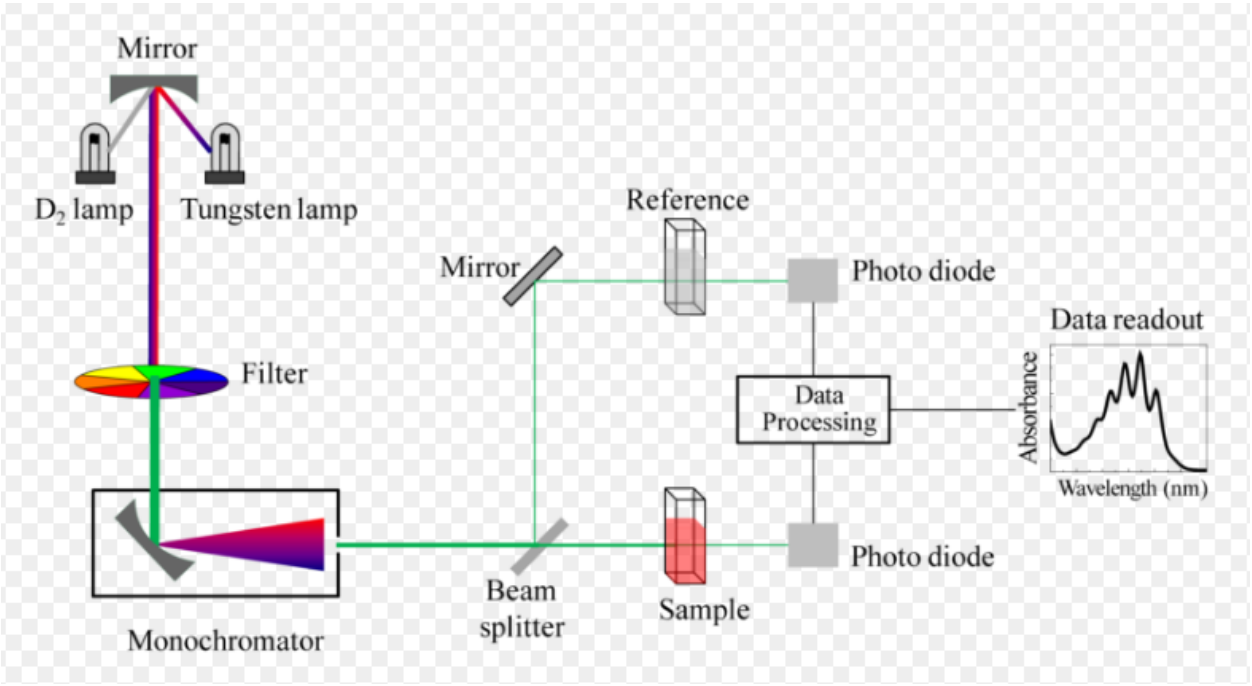

Figure 2.2: Schematic representation of UV-visible spectrophotometer (www.wikimedia.com).

The functioning of this instrument is relatively straight forward. A beam of light from a visible or UV light source is separated into its component wavelength by a prism or diffraction grating. Each monochromatic (single wavelength) beam in turn is split into two equal intensity beams by a half-mirrored device. One beam, the sample beam, passes through a small transparent container (cuvette) containing a solution of the compound being studied in a transparent solvent. The other beam, the reference, passes through an identical cuvette containing

only the solvent. The intensities of these light beams are then measured by electronic detectors and compared. The intensity of the reference beam, which should have suffered little or no light absorption, is defined as I_0. The intensity of the sample beam is defined as I. over a short period of time; the spectrometer automatically scans the entire component wavelength in the manner described.

Transmittance (T) which does not depend on changes of the incident light intensity is obtained using equation (2.5).

$$T = {}^{I}/_{I_o} \tag{2.5}$$

The absorption coefficient (α) for a uniform medium can be defined in terms of the intensity change of a monochromatic light beam in a unit distance that the beam travelled in the medium by (Meyer-Arendt, 1995) as in equation (2.6).

$$\frac{dl}{dx} = -\propto l \tag{2.6}$$

Therefore, the beam intensity as a function of the distance, x, in equation (2.7),can be written as

$$I = I_o e^{-\propto x} \tag{2.7}$$

The absorbance (A) defined in equation (2.8) as:

$$A = -logT \tag{2.8}$$

Absorption may be presented as transmittance (T) or absorbance (A). If no absorption has occurred, T=1 and A=0.

It is therefore clear that the absorbance and absorption coefficient are proportional to one another.

2.7 Solar cell I-V measurement system

Solar simulation used in solar cell performance measurement since solar radiation is not always available and its magnitude differs according to location and surrounding. This system includes a light source, measurement electronics, computer, and software needed to measure solar cell I-V curves. The illumination current versus voltage (I-V) characteristics of photovoltaic device

typically measured with respect to standard reference conditions, defined by a spectrum, intensity, temperature and area. Once the solar simulator intensity has been set to match the standard intensity and spectrum using a reference cell for the particular device being evaluated the I-V characteristics can be measured. The schematic diagram of solar simulator is shown in figure 2.3. A I-V measurement system measures I-V curves of solar cells and calculate critical cell performance parameters including short circuit current (I_{sc}), open circuit voltage (V_{oc}), fill factor (FF), maximum current (I_{max}), maximum voltage (V_{max}), maximum power (P_{max}), efficiency (η), and saves test data in text files foe using it to characterize the cell.

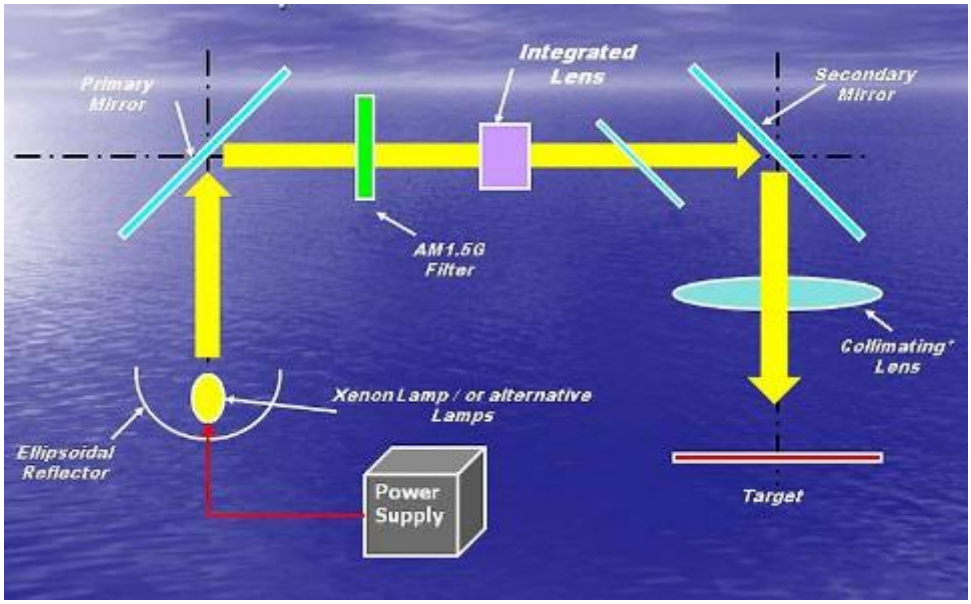

Figure 2.3: Schematic representation of solar cell simulator and I-V measurement system (en.wikipedia.org).

2.8 The properties of DSSCs

- Absorption: the dye should absorb light at wavelengths up to about 920 nm, which is the energy of the excited state of the molecule should be about 1.3 eV above the electronic ground state corresponding to the ideal band gap of a single band gap solar cell (Green, 2005).

- Kinetics: this involves the process of electron injection from the excited state to conducting band of the semiconductor. The process should be fast enough to escape competing unwanted relaxation and reaction pathways.
- Stability: the adsorbed dye molecule should be stable enough in the working environment to sustain about 20years of operation at exposure to natural day light (Gratzel, 2003).

2.9 Theoretical Issues of the DSSC Operation

The need for unique theoretical consideration of the PV effect in DSSCs arises from the fundamental differences in the operation between the DSSCs and the traditional semiconductor p-n junction solar cells.

- In contrast to the semiconductor p-n junction solar cells, where light absorption and charge transport occurs in the same material, the DSSCs separate these functions. Dye molecules absorb photons and transport of charge is carried out in TiO_2 electrode and electrolyte. In conventional solar cells, the semiconductor has the task of light absorption and charge transport, whereas in DSSC the two functions are separately controlled (Pradhan *et al*., 2007).
- Charge separation in the semiconductor p-n junction cells is induced by the electric field across the junction; no such long-range electric fields exist in the DSSCs. The charge separation occurs via other kinds of kinetic and energetic reasons at the dye-covered semiconductor-electrolyte interface.
- In the semiconductor p-n junction cells, the generated opposite charges travel in the same material, while in the DSSCs, electrons travel in the nanoporous TiO_2 network and holes in the electrolyte. This means that the requirement for a pure and defect free semiconductor material in the case of semiconductor p-n junction solar cell is relaxed for the DSSC,

where the recombination can occur only at the semiconductor electrolyte interface.

2.10 Dye-Sensitized Solar Cell Construction

The original design of DSSC by O'Regan and gratzel 2001 has three primary parts. The transparent anode made of fluorine-doped thin dioxide ($SnO_{2:}$ F) deposited on the back of a glass plate. On the back of this conductive plate is a thin layer of TiO_2, which form into a highly porous structure with an extremely high surface area. The plate is then immersed in a mixture of photosensitive ruthernium-polypyridine dye and a solvent. After soaking the film in the dye solution, a thin layer of the dye is left covalently bonded to the surface of the TiO_2. A separate plate is then made with a thin layer of the iodide electrolyte spread over a conductive sheet, typically platinum metal. The two plates are then joined and sealed together to prevent the electrolyte from leaking.

2.11 Construction Procedure

First, begin the process of creating the solar cells with two glass plates coated with FTO or ITO. The plates are first tested to find the conductive side of the glass. This conductive side will be covered with the other materials. TiO_2 is applied to the conductive side of one plate by using a glass rod and rolling it on the plate until a neat coating is achieved. The plate is then placed above a bunsen burner for about 30 min so that the TiO_2 is bonded to the plate. This process is called sintering. Following the sintering process, the plate is allowed to cool and is then placed in a bath of the dye solution for 30 min. After absorbing the dye, the plates are placed to dry and bond. The bottom plate is placed in a hood (conductive side up) so that the counter electrode in the form of the platinum paste may be applied. The electrolyte solution is then placed on the dye side of the plate, enough to saturate the surface. The plates are

sandwiched together (conductive sides touching) and secured with binder clip. The cells are now ready to be tested.

2.12 Dip-Coating

Dip-coating is used for film formation through immersion of substrate in coating solution. After exposure to the solution for a certain period of time, wetting of the substrate surface and subsequent film formation takes place. Following this deposition step is withdrawal of substrate from the solution bath and evaporation of solvent, resulting in formation of film with uniform thickness. Further post-treatment step may be necessary in oder to obtain final coating. Main forces governing dip-coating process are gravitational force, viscous drag, surface tension and force of inertia. (Petrovic *et al*., 2015).

2.13 Spin-Coating

Spin-coating is a well-known, rapid technique used for producing uniform, quality thin films on a variety of substrates. The schematic diagram is represented in figure 2.4. Spin-coating process involves deposition of solution onto a substrate, followed by rotation at high and consequent drying, resulting in a formation of thin film. Thickness of formed film is controlled through several parameters such as viscosity of the solution, temperature and spinning velocity. Post-processing usually includes annealing in order to promote evaporation of residual solvent and improve crystallinity (Yang *et al*., 2004). Spin-coating has advantages of low-cost fast processing, possibility of multiple deposition and small quantities of solution needed for covering large substrate area (Jiang and McFarland, 2004).

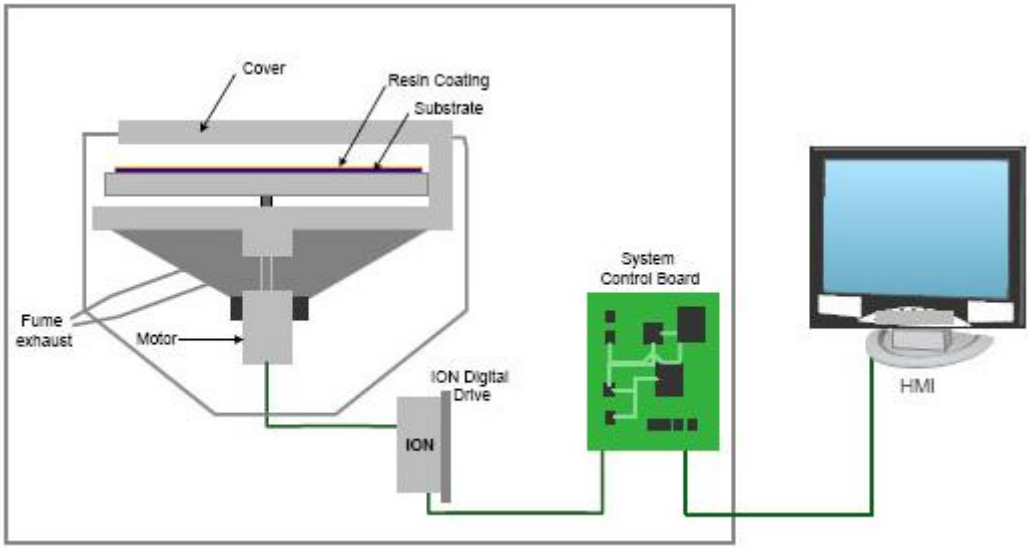

Figure 2.4: Schematic representation of a spin-coater (pmdcorp.com)

2.14 Scanning Electron Microscopy (SEM)

Electron Microscopes are scientific instruments that use a beam of highly energetic electrons to examine objects on a very fine scale. This examination can yield information about the topography (surface features of an object), morphology (shape and size of the particles making up the object), composition (the elements and compounds that the object is composed of and the relative amounts of them) and crystallographic information (how the atoms are arranged in the object) (Voutou and Stefanaki, 2008).

2.14.1 Working principle of SEM

In SEM, a source of electrons is focused in vacuum into a fine probe that is rastered over the surface of the specimen. The electron beam passes through scan coils and objective lens that deflect horizontally and vertically so that the beam scans the surface of the sample as shown in figure 2.5. As the electrons penetrate the surface, a number of interactions occur that can result in the emission of electrons or photons from or through the surface. A reasonable fraction of the electrons emitted can be collected by appropriate detectors, and the output can be used to modulate the brightness of a cathode ray tube (CRT)

whose x- and y- inputs are driven in synchronism with the x-y voltages rastering the electron beam. In this way an image is produced on the CRT; every point that the beam strikes on the sample is mapped directly onto a corresponding point on the screen (R.F Egerton). As a result, the magnification system is simple and linear magnification is calculated by the equation (Voutou and Stefanaki, 2008):

SEM works on a voltage between 2 to 50 kV and its beam diameter that scans the specimen is 5nm-2μm. The principal images produced in SEM are of three types: secondary electron images, backscattered electron images and elemental X-ray maps. Secondary and backscattered electrons are conventionally separated according to their energies. When the energy of the emitted electron is less than about 50eV, it is referred as a secondary electron and backscattered electrons are considered to be the electrons that exit the specimen with an energy greater than 50eV (Brundle, 1992). Detectors of each type of electrons are placed in the microscope in proper positions to collect them.

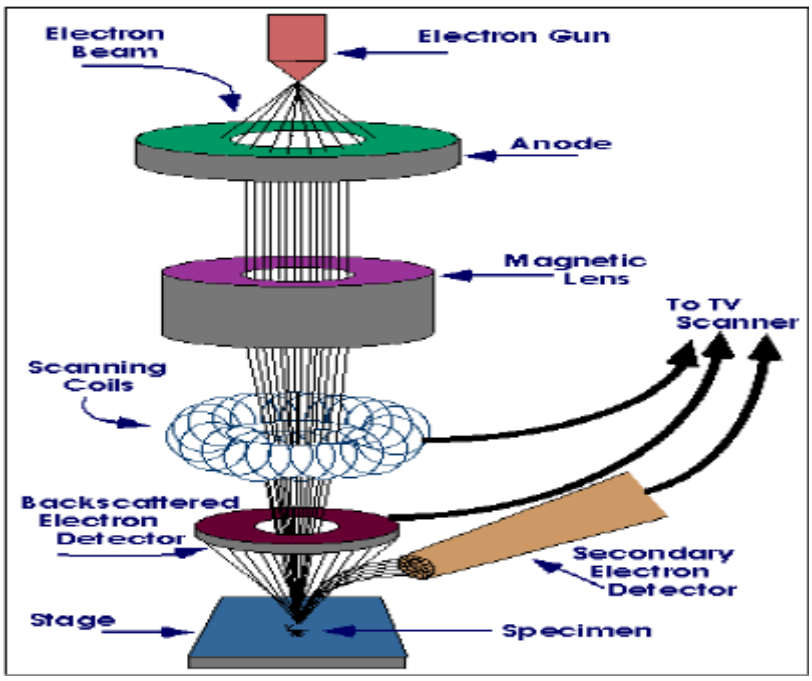

Figure 2.5: Geometry of Scanning Electron Microscopy (Voutou and

2.15 Energy Dispersive X-Ray Spectroscopy (EDX)

EDX is an analytical technique used for the elemental analysis or chemical characterization of a material. It relies on the investigation of an interaction of some source of X-ray excitation and the material. As the electron beam of the SEM is scanned across the sample surface, it generates X-ray fluorescence from the atoms in its path.

CHAPTER THREE

3.0 Materials and Methods

This chapter introduces the different materials and equipments involved in this research. Firstly, the materials used for the DSSC fabrication and device assembly procedures will be analyzed, then the equipments exploited for the characterization of both the materials and the fabricated solar cells will be presented.

3.1 Materials

i. Glass substrates: All the glass plates have transparent conducting oxide (TCO) layer on one side, which make the glasses conductive.

ii. Zinc Oxide (ZnO) solution: this solution is given in a certain quantity to apply it over conductive side of the glass. The solution was made with distilled water and Isopropyl alcohol (IPA).

iii. Dye extract from black cherry, beetroot, paw-paw leaves, yumbo tumtum and Eosin-Y are used as sensitizers.

iv. Multimeter: A multimeter is used to find out the conductive side of the glasses and also measure short circuit current and open circuit voltage, if is connected directly to the DSSC.

v. Pencil: pencil is used to put a graphite layer on the positive electrode of DSSC.

vi. Sonicator: It is used for ultrasonic cleaning of the substrates

vii. Spin coating machine: it is used for deposition of material on a glass substrate.

viii. Tweezers: It is used to pick the substrates and the deposited films.

Other apparatus used are Petri dish, beakers, mortar and pestle, electronic weighing balance, filter paper, hot plate, binder clips, pipette.

Chemicals used are:

i. Ethanol: It is used for cleaning of the substrates and also as solvent.

ii. Isopropyl Alcohol (IPA): It is used to clean the substrates as well as solvent.
iii. Electrolyte (Iodide/Triiodide)
iv. Distilled water: It is used as solvent and also for washing of the substrate materials.
v. Detergent: It is used as a cleaning material.

Equipments used for characterization are:

i. Scanning Electron Microscope (SEM): It is used to determine the morphology of the samples.
ii. UV-VIS Spectrophotometer: It is used to determine the optical properties of the materials.
iii. Solar Simulator: It is used to determine the electrical properties of the fabricated DSSCs.
iv. X-Ray Diffractometer (XRD): it is used structural characterization of a material.

3.2 Methodology

3.2.1 Substrate cleaning

For all the photoelectrodes, FTO coated glasses were used as transparent substrate. Before usage, they were immersed in distilled water with detergent in an ultrasonic bath for 15minutes at 30 ℃ with the help of a VWR ultrasonic cleaner model 07043-986 Symphony. They were then rinsed with distilled water in ultrasonic cleaner at the same condition, later with ethanol at the same condition and lastly, with Isopropyl alcohol at the same condition and dried.

3.2.2 Preparation of the zinc oxide (ZnO) electrodes.

Using twenty five weight percent, 2.5 g of commercial ZnO (Z_1) and biosynthesized ZnO (Z_2) were hydrolyzed at 90 ℃ in 10ml of Isopropyl alcohol

and distilled water of same ratio for 40minutes respectively. The mixtures were well mixed using an ultrasonic heat-stir (Stuart heat-stir UC152). Smooth and milky solutions were obtained. The result paste were deposited on fluorine doped tin oxide (FTO) coated glass using a spin-coating machine (WS-650MZ-23NPP Laurell). The equipment used during ZnO film preparation are shown in plate 3.1.

Weighing machine Electronic stirrer Spin-coating machine

Plate 3.1: Stages in synthesizing ZnO thin films (Materials Science and Engineering Laboratory, Kwara State University, Malete)

The deposited ZnO thin films were dried on a hot plate at 100 ℃ for 1 hour. Later, the films were annealed at 500 ℃ for 1hour in a furnace to increase the adherence between particles and with the TCO layer. Thereafter they were left in the furnace to cool till the next day to avoid cracking of the films. Annealed films of ZnO prepared and treated are shown in plate 3.2.

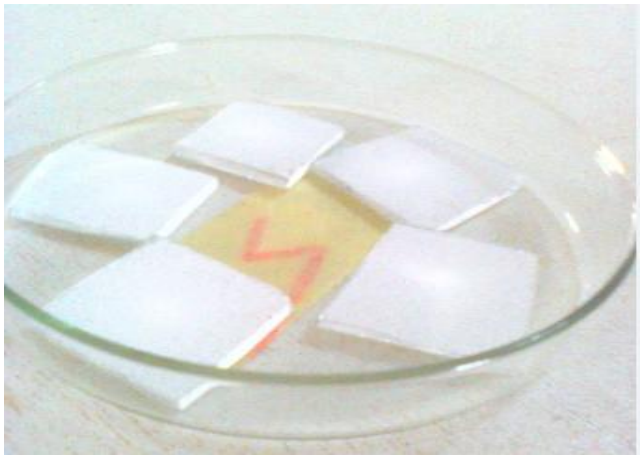

Plate 3.2: Annealed ZnO electrode

3.2.3 Preparation of the dyes:

Pawpaw leaf

The leaves were crushed with mortar and pestle. After which, the dye was squeezed out using a sieve. The leaves of Pawpaw and its dye extract is shown in plate 3.3.

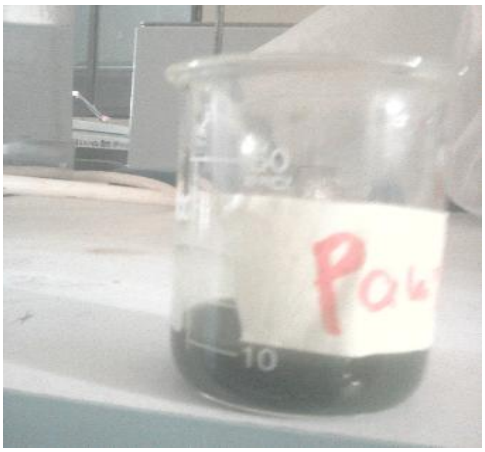

Plate 3.3: Pawpaw leaf and its dye extract

Beetroot

Few tubers were cooked with a water proof material for 30minutes and allowed to cool. Later they were crushed with mortar and pestle. The juice was filtered out using a sieve. Images of Beetroot and its dye extract are shown in plate 3.4.


Plate 3.4: Beetroot and its dye extract

Black cherry

The fruits were crushed in mortar and pestle, and the juice was extracted using a sieve shown in plate 3.5.


Plate 3.5: Black cherry and its dye extract

Yombo Tumtum

The Yombo tumtum powder was weighed (0.8 g) and dissolved with 2ml of ethanol. A smooth dark solution was obtained and image of the dye extract is shown in plate 3.6.

Plate 3.6: Dye from Yombotumtum

Eosin-Y

This synthetic dye was dissolved with Isopropyl alcohol and a smooth solution was obtained. The image of dye extract is shown in plate 3.7.

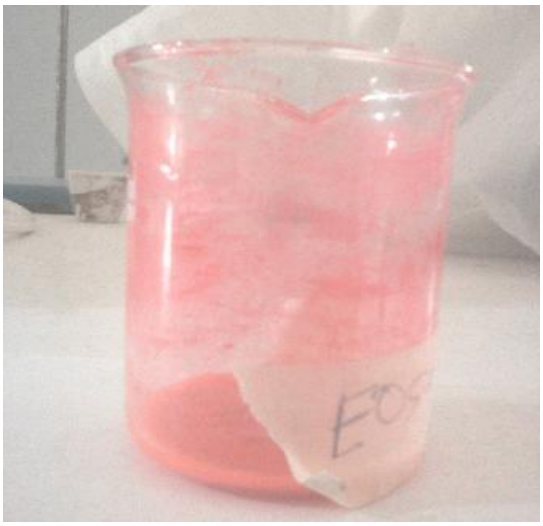

Plate 3.7: Dye from Eosin-Y

3.2.4 The sensitizing process

After cooling, the ZnO electrodes were immersed into the various dye solutions for 18 hours. The dye solutions were covered with aluminum foil to block out light and prevent evaporation. After removing the substrates, they were rinsed with ethanol solution, in order to remove excess dye. Thereafter the ZnO

electrode were left to dry for further characterization. Image of dye films deposited on FTO substrate as shown in figure 3.1.

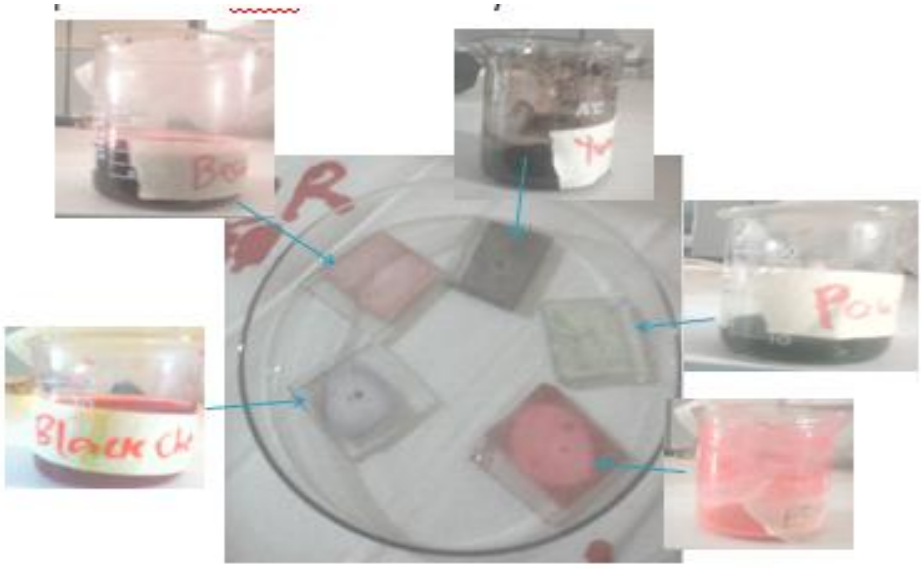

Figure 3.1: Sensitized ZnO electrodes

3.2.5 Preparation of the counter electrode

Counter electrode was done by scratching graphite using pencil on the cleaned FTO glass substrate. The image of coated counter electrode is shown in plate 3.8.

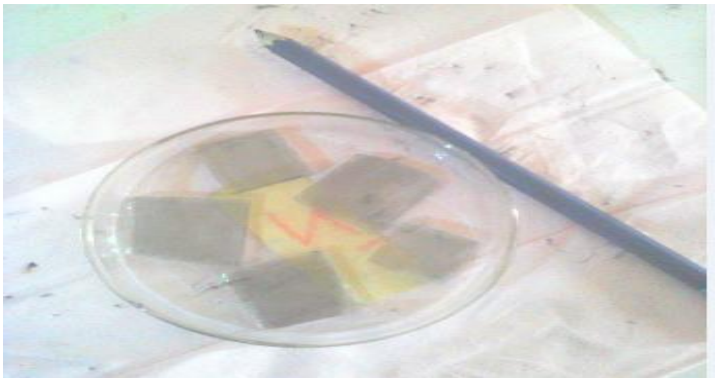

Plate 3.8: Coated counter electrode

3.3 Surface morphology

Morphology analysis was taken for the ZnO electrode. This examination revealed the morphology (shape, size, porosity and uniformity of the grains) of

the ZnO thin film. The SEM machine used (EVO/LS10 ZEISS) is shown in plate 3.9.

Plate 3.9: Scanning Electron Microscope (SEM) with EDS (African Development Bank Laboratory, African University of Science and Technology, Abuja)

3.4 Optical characterization

After the extraction of the dyes, the absorption spectrums of the dyes were observed and were recorded using a UV-VIS Spectrophotometer (UV-6705UV/VIS spectrophotometer, JENWAY) as in plate 3.10.

Plate 3.10: UV-VIS Spectrophotometer (Materials Science and Engineering Laboratory, Kwara State University, Malete)

FTIR spectroscopy measurements were carried out on a Thermo Scientific (iS5 Nicolet) as in plate 3.11 using KBr pellets.

Plate 3.11: FTIR machine (African Development Bank Laboratory, African University of Science and Technology, Abuja)

3.5 Structural characterization of the ZnO

X-Ray diffractometer (Brucker, D8 Advance) was used to examine the structural properties of the biosynthesized ZnO. The image of the machine is shown in plate 3.12.

Plate 3.12: XRD machine (African Development Bank Laboratory, African University of Science and Technology, Abuja)

3.6 Assembling of the DSSCs

DSSCs were assembled following the schematic diagram described in figure 3.2, the catalyst- coated counter electrode on the top so that the conductive side of the counter electrode faces the Zinc oxide film.

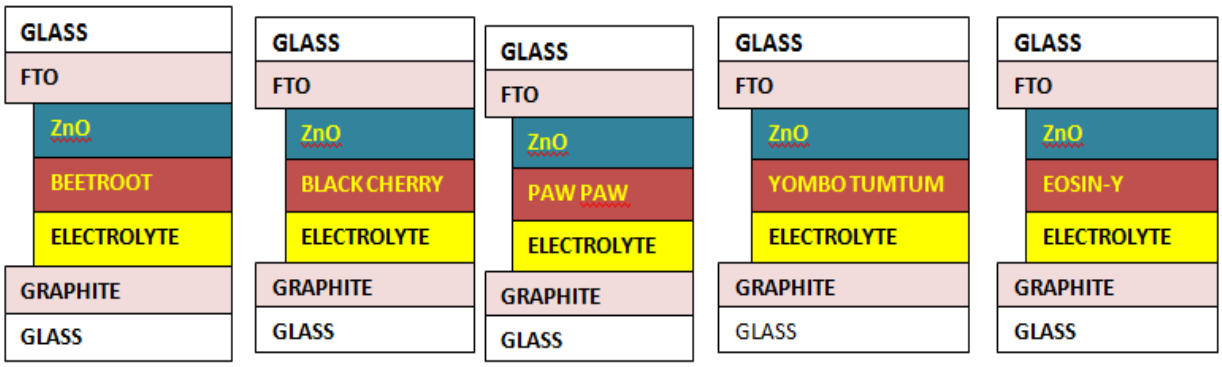

Figure 3.2: Configurations of the DSSCs

The electrolyte solution (Iodide/triiodide) was placed at the edges of the plates. The liquid electrolyte was drawn into the space between the electrodes by capillary action. Binder clips were used to hold the electrodes together. The fabricated solar cells are shown in figure 3.3 below.

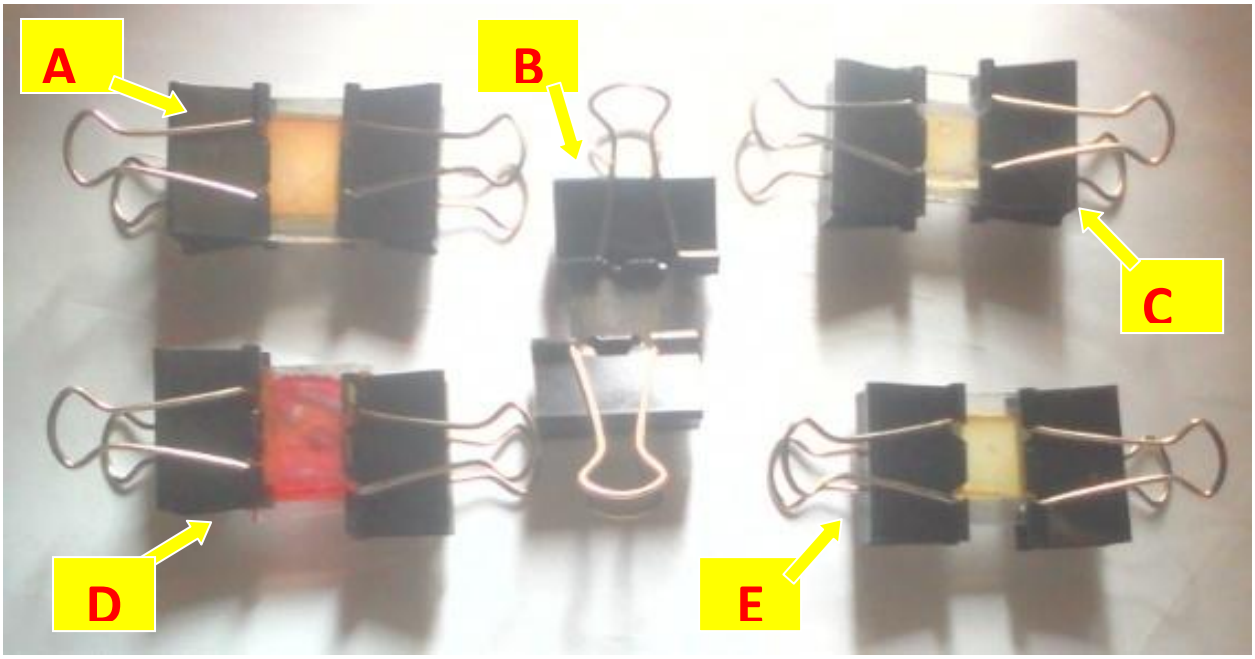

Figure 3.3: Fabricated and assembled DSSCs from (A) Beetroot (B) Yombo tumtum (C) Black Cherry (D) Eosin-Y (E) Pawpaw leaf.

3.7 Electrical characterization

A solar simulator, under the irradiation of AM 1.5 ($100mWcm^{-2}$) shown in plate 3.13 below was used to determine the characterization parameters of the solar cells (DSSCs) which gave rise to the graph used to obtain maximum current (I_{max}), maximum voltage (V_{max}), short circuit current (I_{sc}) and open circuit voltage (V_{oc}).

Plate 3.13: Solar simulator (African Development Bank Laboratory, African University of Science and Technology, Abuja)

CHAPTER FOUR

4.0 Results and Discussion

4.1 Introduction

This chapter deals with results and discussion of characterized thin films, extracted dyes and fabricated solar cells. Thin films are ZnO of two types: commercial ZnO (Z_1) and biosynthesized ZnO (Z_2). Optical, micro-structural (morphology), Fourier Transform Infrared Spectroscopy (FTIR) and structural analyses of Z_2 thin films were carried out using UV-Vis spectrophotometer for transmittance and absorrptio properties, Scanning Electron Microscopy (SEM) equipped with Energy Dispersive X-ray (EDX) for capturing the images containing topological information of thin films and elemental composition, FTIR machine for identifying chemical groups and bonds and XRD for studying the crystal structure of ZnO, respectively. Z_1 was only characterized using SEM. Optical properties of extracted dyes were characterized using UV-Vis spectrophotometer. Solar simulator was used to characterize the performance of the fabricated solar cells.

4.2 Properties of ZnO Thin Films as Photo-anode

This section entails the optical, morphology, elemental composition, chemical groups and bonds, and structural characterization of Z_2 from bitter leaf and morphology of Z_1 as photo-anodes.

4.2.1 Optical properties of biosynthesized ZnO (Z_2)

Absorption and transmittance spectra of the sample are as shown in figures 4.1 and 4.2. The sample was characterized at visible regions (400 – 770 nm). The sample has low of absorption of visible light at the said wavelength region. It shows that it has average absorption of 21.7980 % at visible region. Also, the transmittance at wavelength of 300 to 800 nm shows that the offset transmission by the material is at region 320 nm which corresponds to optical energy gap of 3.88 eV. This shows that this material allows transmission of all visible light

incidents on it. The calculated average transmittance of biosynthesized ZnO is 41.63 % as shown in figure 4.2.

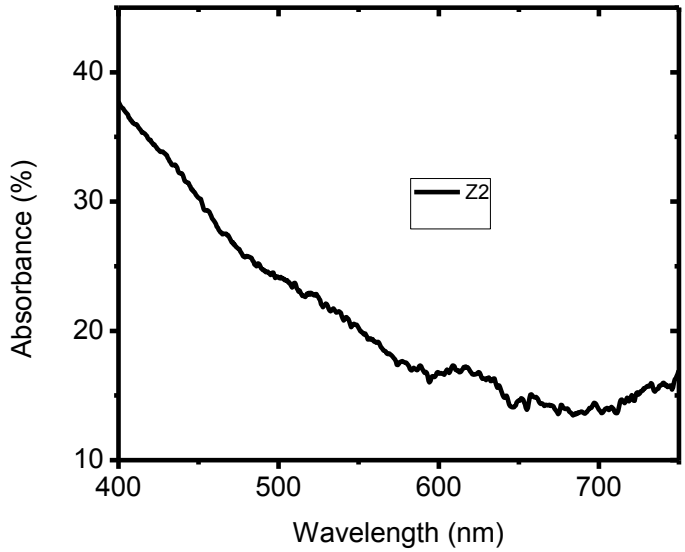

Figure 4.1: Absorption spectrum of biosynthesized ZnO

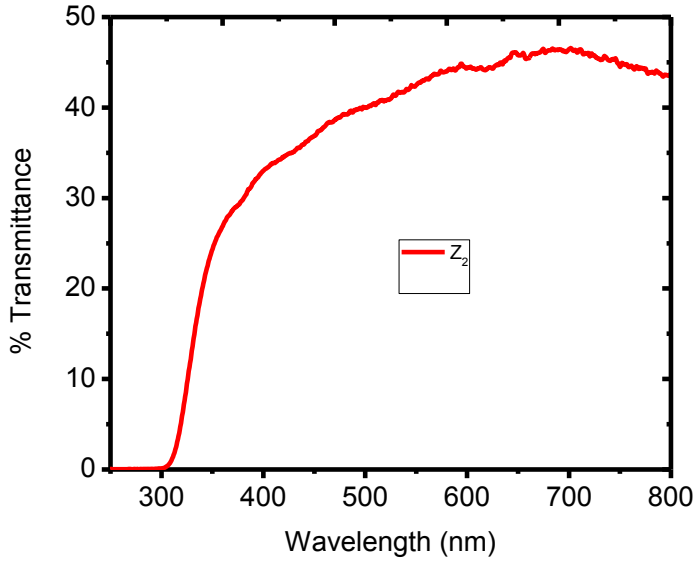

Figure 4.2: transmittance spectrum of biosynthesized ZnO

4.2.2 Surface morphology characterization

Plates 4.1 and 4.2 show the morphologies of the ZnO thin films (Z1 and Z2, respectively) deposited by solution method as evaluated by scanning electron microscope (SEM). The image of the ZnO thin films prepared have pores which

allow electrons to travel and be collected at the conducting substrate. The heat treatment of ZnO reduces voids of the film layer so as to increase the quality of ZnO particle in a unit area of the film, thus enhancing the adsorptive capability of the natural dye molecules. The SEM reveals that the particles are spherical and have granular nature. The morphology of the films shows that both films are uniformly distributed on substrate. The uniform distributed films in both sample reduced short circuiting in solar cells.

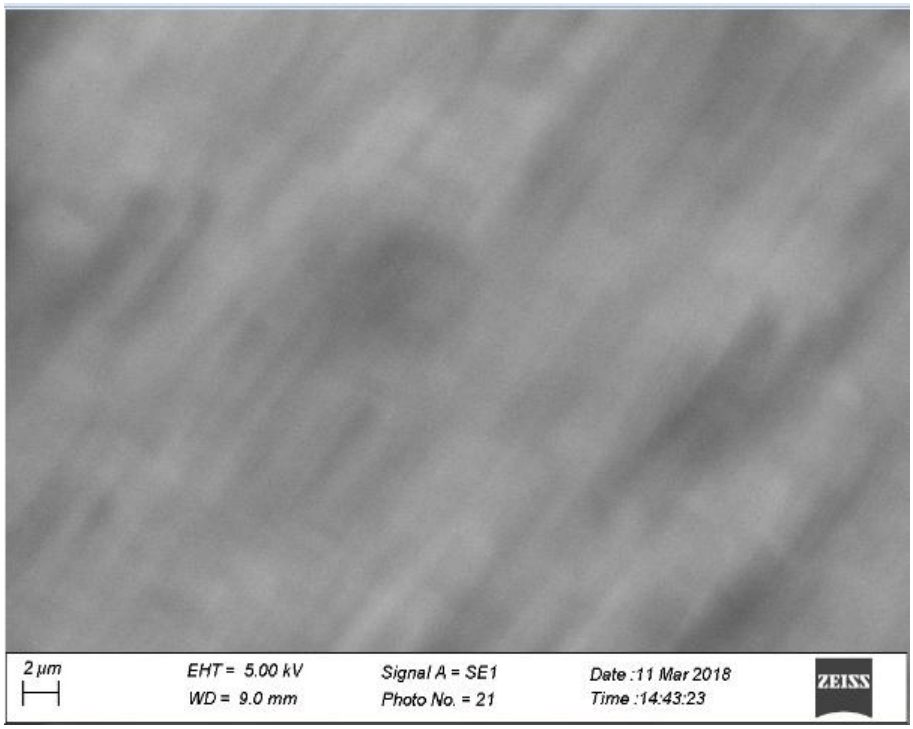

Plate 4.1: SEM analysis of commercial ZnO (Z_1) thin film.

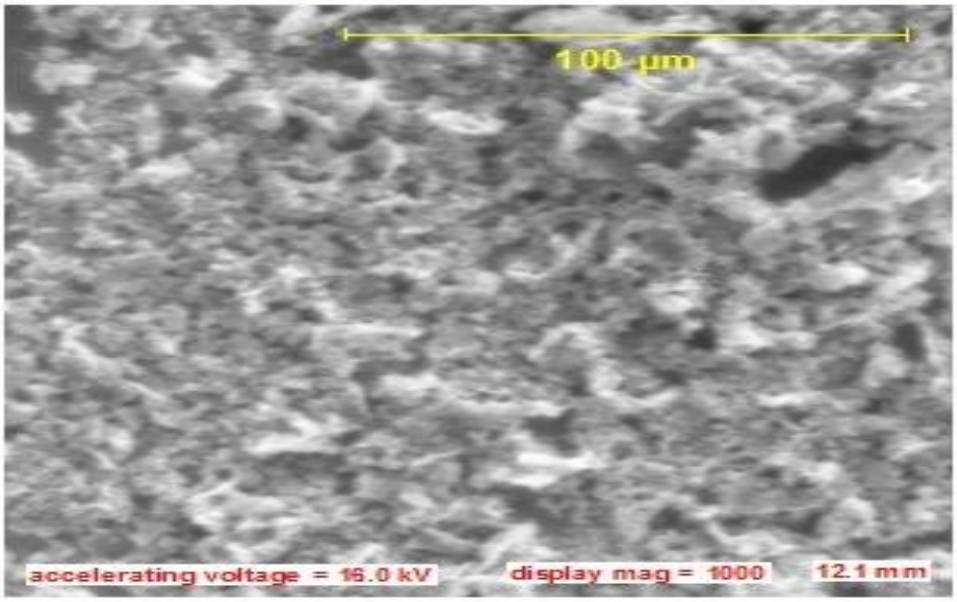

Plate 4.2: SEM analysis of synthetic ZnO (Z_2) thin film.

4.2.3 Energy Dispersive X-Ray (EDX)

Figure 4.3 shows the analysis of the elemental composition of biosynthesized ZnO compound (Z_2) using Energy-Dispersive X-ray (EDX). The EDX analysis shows that the compound composed of zinc and oxygen. Zinc has 82.32 weight %, 53.27 atomic % and oxygen has 17.68 weight %, 46.74 atomic %. The revelation of elemental composition of the sample shows that zinc and oxygen are present which confirm that ZnO was actually deposited.

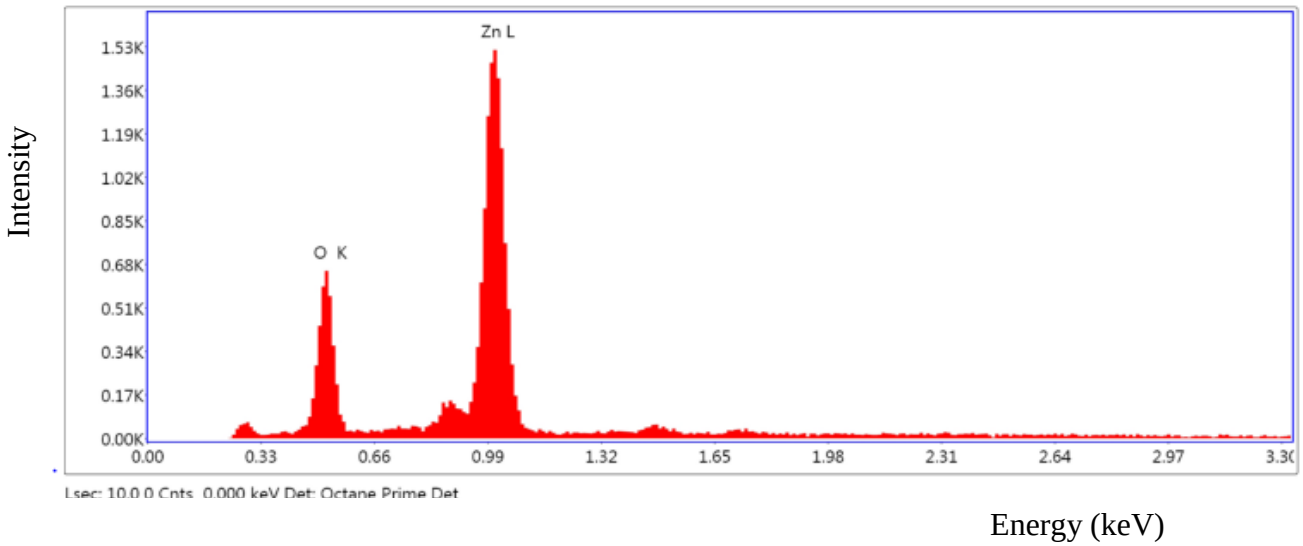

Figure 4.3: Elemental composition of ZnO (Z_2)

4.2.4 FOURIER TRANSFORM INFRARED SPECTROSCOPY (FTIR)

The FTIR spectrum of Z_2 was recorded on (model) spectrometer using KBr pellet technique in the range of 400 – 4000 cm^{-1}. The identification of the atomic arrangement and the concentrations of the chemical bonds present in the samples have been carried out using Fourier Transform Infra-red Spectroscopy (FTIR), in which percentage transmission and wave number are the output. The FTIR spectrogram of biologically synthesized ZnO with bitter leaf (Z2) is shown in Figure 4.4. The peaks at 3400 cm^{-1} is due to N-H stretching in aliphatic amines, the peak at 1650 cm^{-1} is due to N-H bonding in the compound type of 1^0 amines, the peak at 1380 cm^{-1} is due to the presence of inorganic nitrate ion and the peak at 1050 cm^{-1} is due to the presence of C-N stretching in aliphatic amines.

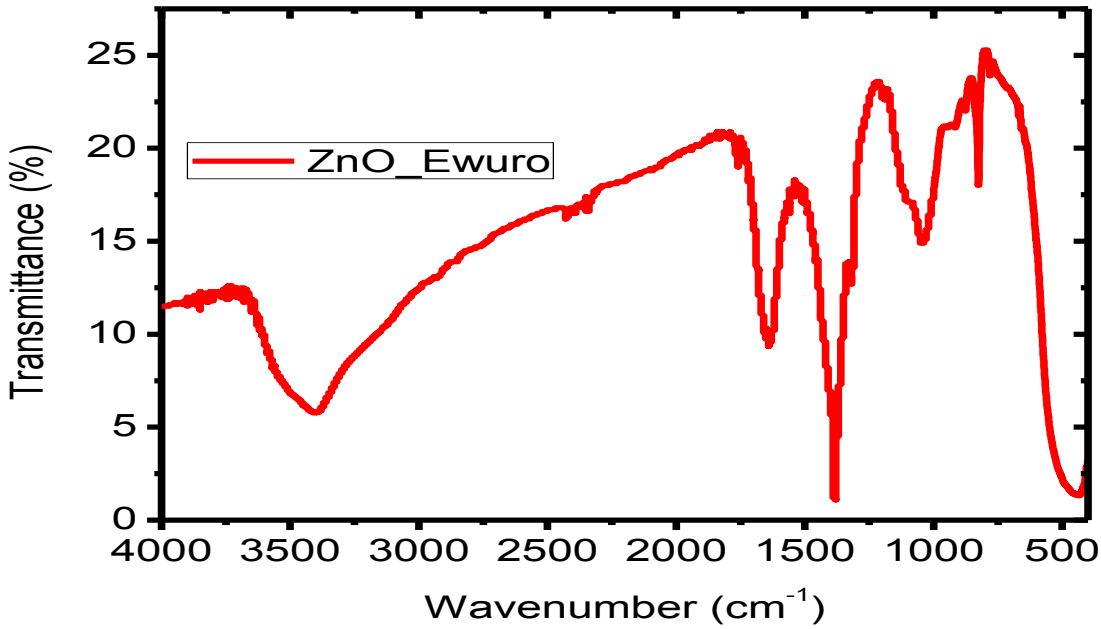

Figure 4.4: FTIR spectrum of biosynthesized ZnO (Z_2)

4.2.5 X-RAY Diffractometry (XRD) analysis

The XRD of ZnO (Z_2) synthesized with bitter leaf is as shown in figure 4.5. According to the spectrogram of the crystal structure, the well defined peaks typical of ZnO in the crystal structure

are clearly noticed. The peaks are in well defined shape and form. This indicates the crystallinity of the synthesized ZnO nanoparticles. The peaks are indexed as $31.67°\ (100),\ 34.28°(002),\ 36.43°(101),$ and $47.48°\ (102)$, respectively. All diffraction peaks of the sample correspond to the characteristic hexagonal wurtzite structure of zinc oxide nanoparticles ($a = 0.315\ nm$ and $c = 0.529\ nm$) [Kumar and Rani, 2013]. Average particle size of ZnO nanoparticle is found to be $9.5\ nm$ according to Scherrer equation [Culity, 1987]. Also, the analysis of ZnO nanoparticle showed that weight percent of 80.34 and 19.66 correspond to zinc and oxygen, respectively. This corresponds to the result gotten from EDX and confirms that ZnO was synthesized.

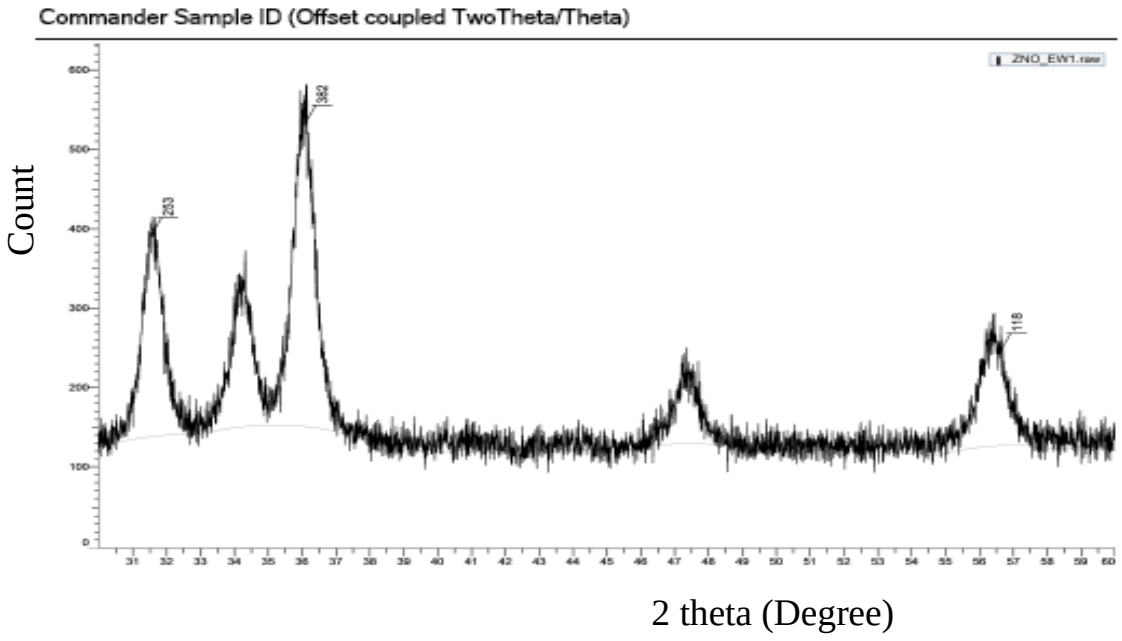

Figure 4.7: XRD patterns of biosynthesized ZnO(Z_2)

4.3 Optical analysis of active materials (Dyes)

Figure 4.6 – 4.11 present the absorption spectra obtained for the different dyes extracts. Different dyes show different absorption wavelength due to differences in composition (Bisquert et al., 2004, Hara et al. 2004). Absorption peak of Pawpaw dye extract occurred at 580 nm with offset absorption value of 472 nm

as shown figure 4.6. Absorbance increases with wavelength from the offset absorption value. The offset absorption value corresponds to optical energy band gap of 2.63 eV. Absorption peaks of Black cherry, Beetroot, Yombotumtum and Eosin-Y correspond to wavelengths of 525, 510, 562 and 540 -575 nm, respectively as shown in figures 4.7 – 4.10. Offset absorption values of Black cherry, Beetroot, Yombotumtum and Eosin-Y correspond to 692, 562, 682 and 698 nm, respectively. The average absorbance of different dyes is shown in table 4.1. The optical band gap of the beetroot, pawpaw leaf, black cherry, yombo tum tum and Eosin-Y was determined from the absorption spectra using the relation, $E_g = \frac{1240}{\lambda\,(nm)}$. The table 4.2 shows wavelength and its corresponding band gap values of the dyes. The optical energy band gaps of beetroot, pawpaw leaf, black cherry, Yombotumtum and Eosin-Y are 2.21, 2.63, 1.79, 1.82 and 1.78 eV, respectively. These show that the dyes absorb visible light which is essential for every active material in solar cells. The combined plots of the absorption behaviors of dyes with wavelength are shown in figure 4.11. There is red-shift in absorption peaks from the dye of Beetroot, Black Cherry, Eosin-Y, Yombotumtum to Pawpaw leaf.

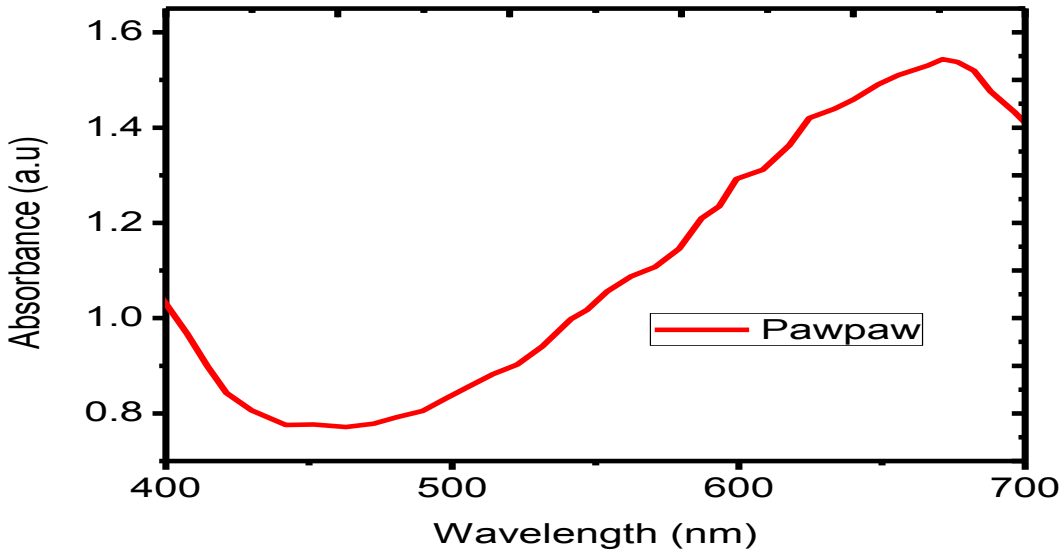

Figure 4.6: Plot of absorption spectrum of Pawpaw leaf dye extract.

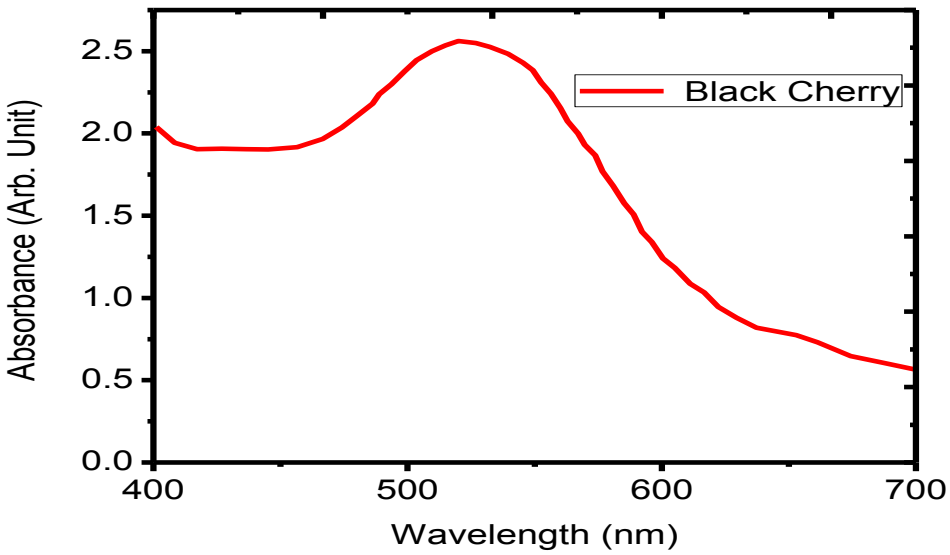

Figure 4.7: Plot of absorption spectrum of Black Cherry dye extract.

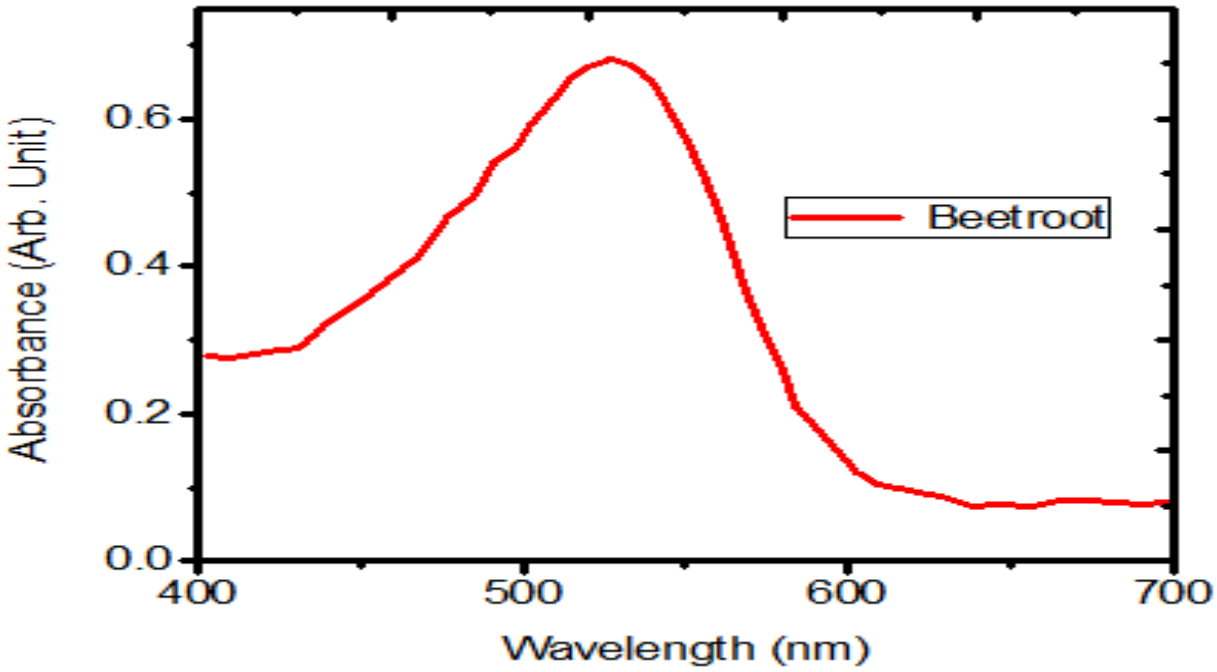

Figure 4.8: Plot of absorption spectrum of Beetroot dye extract.

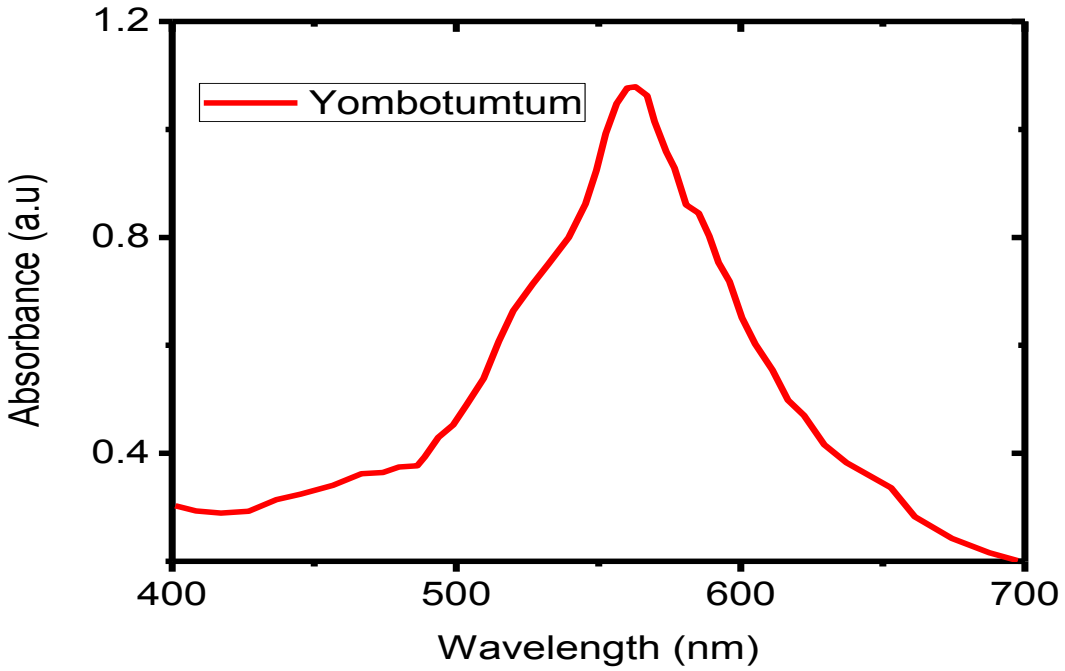

Figure 4.9: Plot of absorption spectrum of Yombotumtum dye extract.

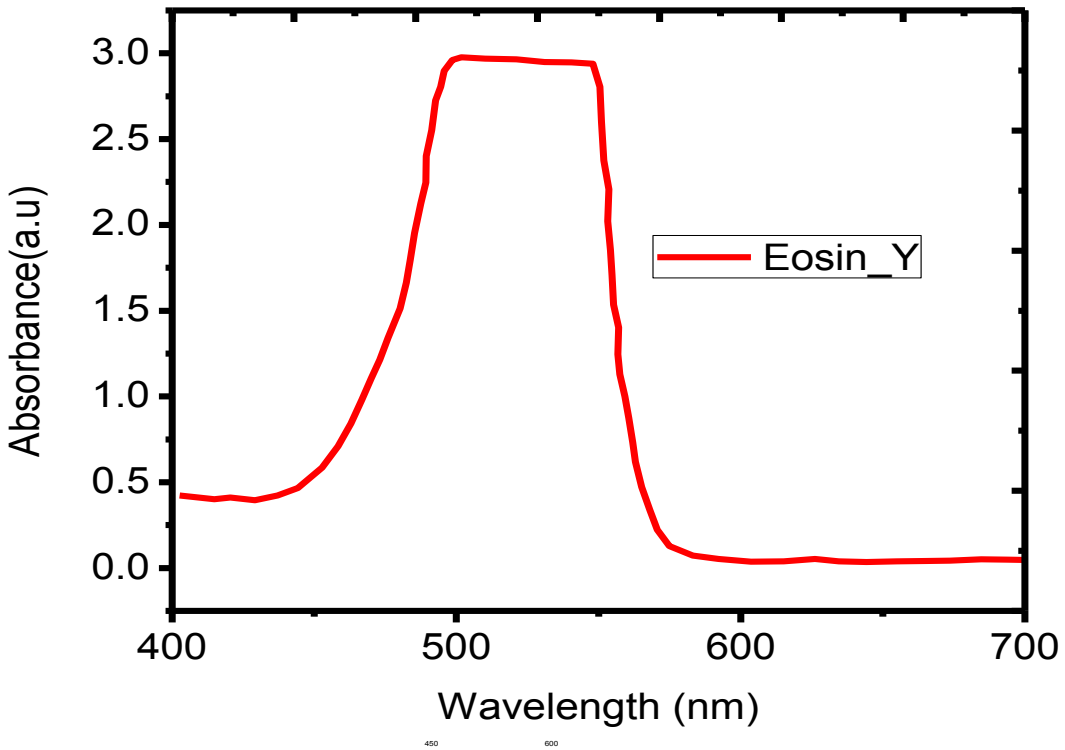

Figure 4.10: Plot of absorption spectrum of Eosin_Y dye extract.

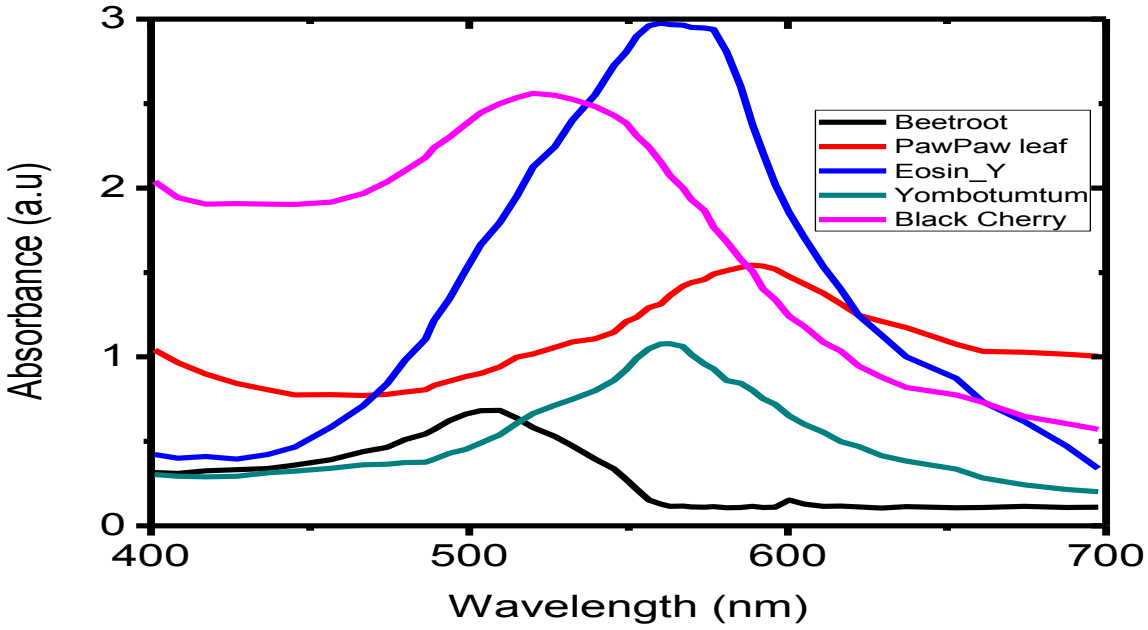

Figure 4.11: Plot of absorption spectrum of all Dye extracts

Table 4.1: Average absorbance of various extracted dyes

S/N	Dye extract	Average Absorbance (a.u)
1	Beetroot (B_d)	0.2872
2	Pawpaw leaf (P_d)	1.1319
3	Eosin_Y (E_d)	1.6585
4	Yombotumtum (Y_d)	0.5886
5	Black Cherry (CS_d)	1.7814

Table 4.2: Energy band gap of the dyes

Dye	Offset absorption wavelength (nm)	E_g (eV)
Pawpaw leaf (P_d)	472	2.63
Beetroot (B_d)	562	2.21
Black Cherry (CS_d)	692	1.79
Yombotumtum (Y_d)	682	1.82
Eosin-Y (E_d)	698	1.78

4.4 The current-voltage (I-V) characterization

The cells fabricated from each of the dyes were subjected to photoelectric characterization. Active area of the fabricated solar cells is 4 cm^2. The smooth I-V curves shown in figure 4.12 – 4.19 are the products of solar cells fabricated as shown in figure 3.3 in chapter three. The solar cells parameters (short circuit current (I_{sc}), Open circuit voltage (V_{oc}), Fill factor (FF) and efficiency (η) are generally low. The η, V_{oc}, I_{sc} and FF of the DSSC prepared by Pawpaw leaf are 0.68 %, 0.4140 V, 18.28 mA and 0.3594, respectively. Black Cherry, using commercial ZnO powder (Z_1), has η, V_{oc}, I_{sc} and FF of 0.703 % 0.4147 V 18.05 mA and 0.37562, respectively. The values of data obtained from I-V measurement for both Pawpaw leaf and Black cherry dyes based DSSCs are shown in table 4.3. Beetroot has η, V_{oc}, I_{sc} and FF of 0.430 %, 0.4147 V, 11.03 mA and 0.37579, respectively. I-V measurement values of Beetroot dye based DSSC is shown in table 4.4. Yombotumtum has η, V_{oc}, I_{sc} and FF of 0.528% 0.391 V, 15.41 mA and 0.35019. I-V measurement values of Yombotumtum dye based DSSC is shown in table 4.5. However, η of the synthetic dye Eosin-Y DSSC which serves as standard in this work was 1.161 % with V_{oc}, I_{sc} and FF of 0.4607 V, 22.9 mA and 0.44000, respectively. Among all the solar cells fabricated using commercial ZnO based and natural dyes as the active materials, Black Cherry based solar exhibits highest efficiency of 0.703 %. Solar cells parameters obtained from I-V curves in figures 4.12 – 4.19 show that the cells have high series resistance (R_s) and very low values of shunt resistance (R_{sh}). Very high values of series resistance (R_s) and very low values of shunt resistance (R_{sh}) reduce short-circuit current (I_{sc}) and open-circuit voltage (V_{oc}), respectively. This could be from sum of the contact resistance on the front and back surfaces and the Ohmic resistance of the bulk and n^+ (and p^+) diffused layers on the front (and back) sides. Also, imperfections on the device surface and the bulk as well as from leakage currents across the edge of the cell could

affect the cells performance. Increase in leakage current by shunt resistance lowers the maximum output (P_{max}), V_{oc} and FF [Singh and Ravindra, 2011]. Thereafter, solar cell based on Z_2 (ZnO synthesized from bitter leaf) fabricated using optimized dye (Black Cherry, as shown in figure 4.17, and compared with Z_1 (commercial ZnO powder) using the same dye. Both cells have the same I_{sc} of 18.05 mA but different V_{oc} as in figure 4.18, of 0.4147 and 0.3900 V for Z_1 and Z_2, respectively. The values of data obtained from I-V measurement for both Eosin-Y and Black cherry (Z_2) dyes based DSSCs are shown in table 4.6. Decrease in V_{oc} as seen in Z_2 could be attributed to very high series resistance of the cell. In addition, imperfection on the film surface could lead to lower V_{oc} in the cell. The η of Z_1 and Z_2 are 0.703 and 0.627 %. Figure 4.19 shows the I-V curve of all dyes based solar cells. The values of data obtained from I-V measurement for compared Z_1 and Z_2, and All dyes used as active materials are shown in tables 4.7 and 4.8, respectively.

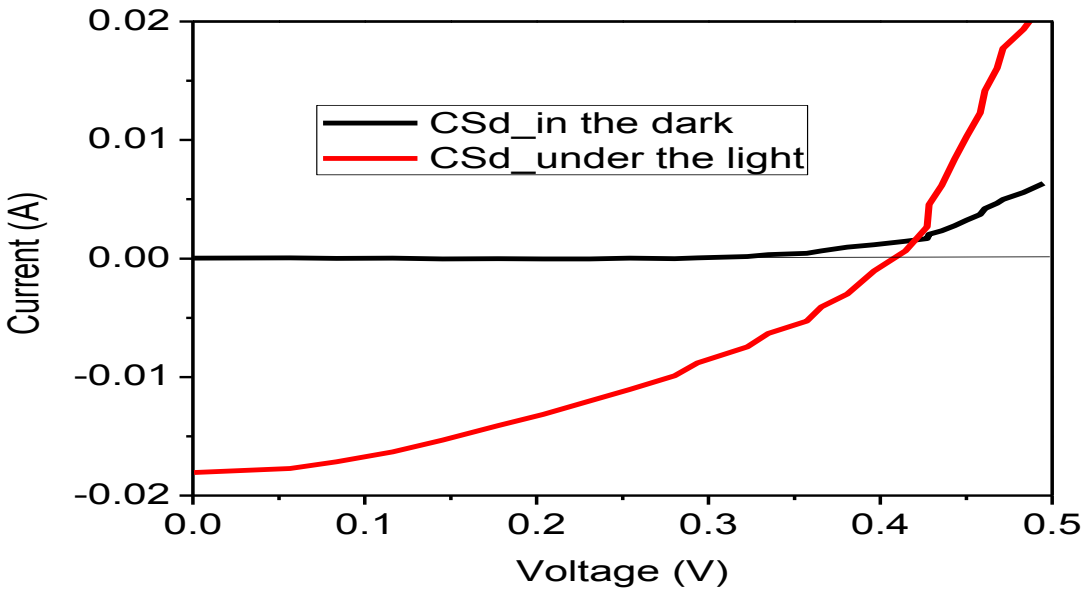

Figure 4.12: Dark and illuminated I-V curves from the fabricated black cherry DSSC based on commercial ZnO (Z_1)

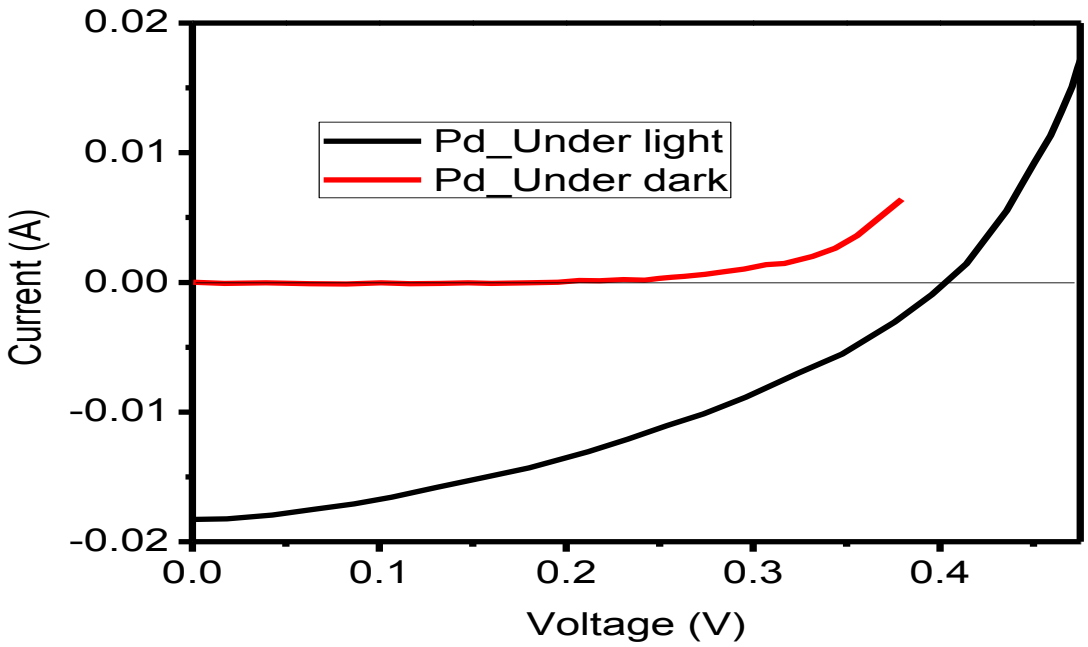

Figure 4.13: Dark and illuminated I-V curves from the fabricated pawpaw leaf DSSC

Table 4.3: I-V values of black cherry dye on commercial ZnO powder (CSd) and Pawpaw leaf dye (Pd) based DSSCs

Voltage (V)	Current (A)	Current (A)	Voltage (V)	Current (A)	Current (A)
	CSd_in the dark	CSd_under the Light		Pd_Under light	Pd_in the dark
7.24138E-4	3.14936E-5	-0.01805	2.65048E-4	-0.01828	1.21138E-6
0.05656	5.36093E-5	-0.01772	0.01851	-0.01824	-8.60889E-5
0.08344	5.56656E-6	-0.01716	0.04281	-0.01795	-3.64222E-5
0.11619	2.43724E-5	-0.01632	0.06437	-0.01752	-1.09186E-4
0.14539	-2.36703E-5	-0.01532	0.08661	-0.01708	-1.26791E-4
0.17754	-4.31281E-6	-0.01409	0.1068	-0.01657	-2.31778E-5
0.20383	-2.30686E-5	-0.01314	0.13034	-0.01581	-1.12901E-4
0.2309	-3.68595E-5	-0.01202	0.13034	-0.01581	-7.65594E-5
0.2543	4.16237E-5	-0.01106	0.1559	-0.01506	-4.26406E-5

0.28041	-3.10924E-6	-0.00988	0.18011	-0.0143	-7.72056E-5
0.29361	5.10517E-5	-0.0088	0.21168	-0.01307	-5.66117E-5
0.32259	1.69303E-4	-0.00744	0.23315	-0.01209	-3.35956E-5
0.33486	3.17944E-4	-0.00631	0.25393	-0.01103	2.74579E-6
0.35725	4.37299E-4	-0.00529	0.27339	-0.01014	1.53038E-4
0.36563	6.55556E-4	-0.00409	0.29615	-0.00884	1.14839E-4
0.38083	9.66667E-4	-0.00299	0.32423	-0.00699	2.06338E-4
0.39645	0.00116	-0.00106	0.34765	-0.00554	1.69351E-4
0.41466	0.00147	6.42438E-4	0.37563	-0.00307	3.11163E-4
0.42726	0.00169	0.00268	0.39554	-9.31034E-4	3.89338E-4
0.42826	0.00204	0.00457	0.41407	0.00144	4.66301E-4
0.43559	0.00235	0.00617	0.43568	0.00553	6.16667E-4
0.44317	0.00276	0.00839	0.44346	0.00749	8.27778E-4
0.4503	0.00324	0.01033	0.45059	0.00929	0.00104
0.45816	0.00372	0.01229	0.45903	0.01132	0.00138
0.46079	0.00423	0.01417	0.46481	0.01312	0.00146
0.46801	0.00468	0.01606	0.47057	0.01508	0.00199
0.47148	0.00499	0.01774	0.4737	0.01657	0.00264

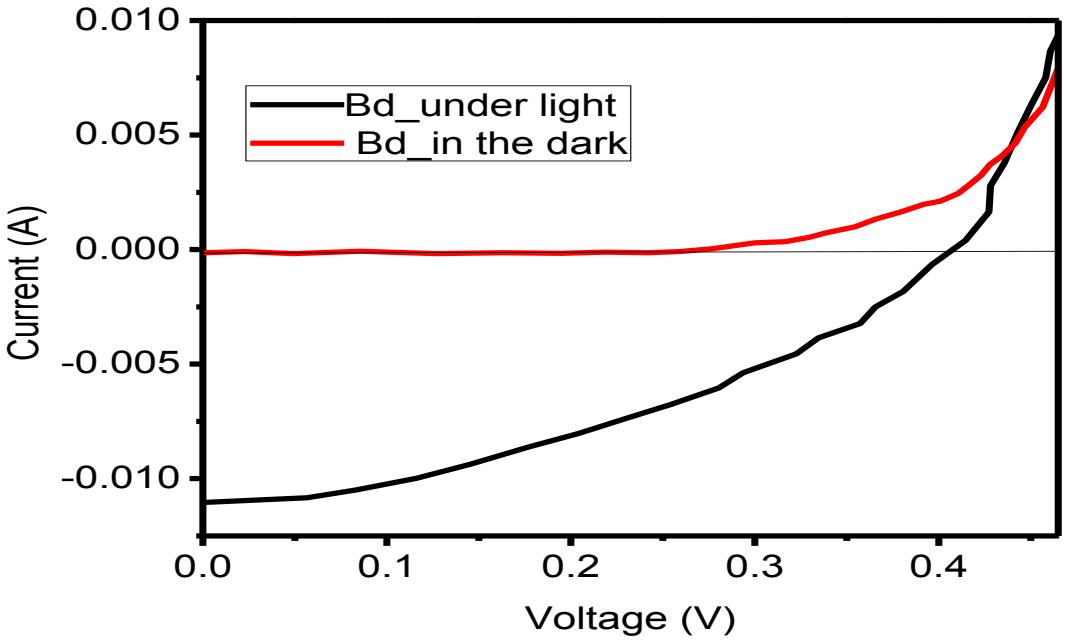

Figure 4.14: Dark and illuminated I-V curves from the fabricated beetroot DSSC

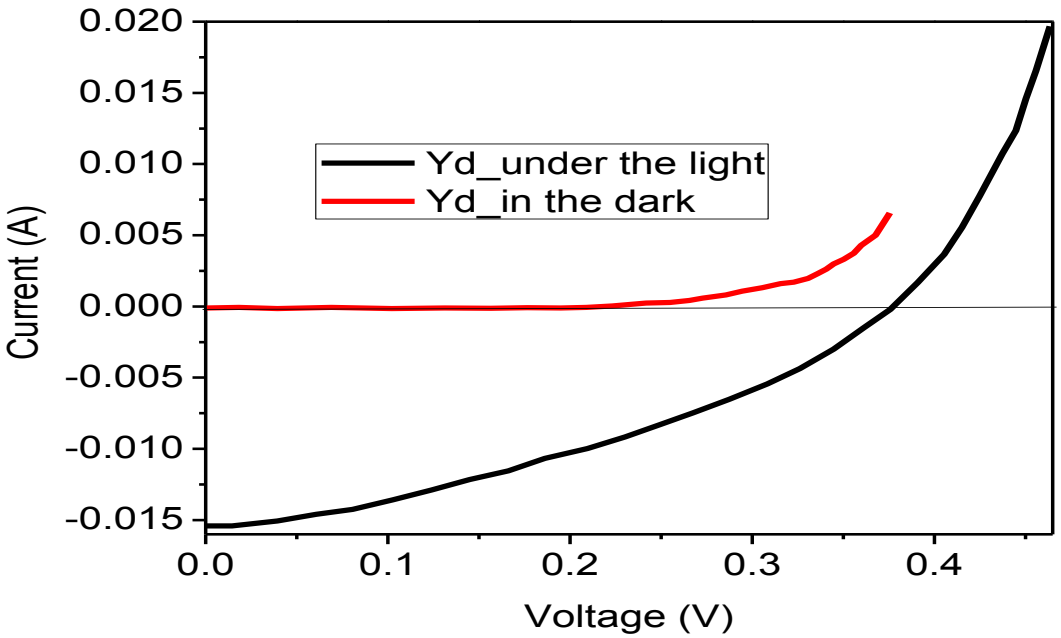

Figure 4.15: Dark and illuminated I-V curves from the fabricated Yombotumtum DSSC

Table 4.4: I-V values of Beetroot dye (Bd) based DSSC

Voltage (V)	Current (A)	Current (A)
	Bd_in the dark	Bd_under the light
-0.00267	4.62462E-6	-0.00102
0.03474	1.92692E-7	-9.78723E-4
0.08285	5.01918E-6	-9.3617E-4
0.12027	5.21187E-6	-9.14894E-4
0.15501	5.42291E-6	-8.7234E-4
0.19243	1.48648E-5	-8.08511E-4
0.22717	2.42609E-5	-7.23404E-4
0.26726	4.75491E-5	-6.17021E-4
0.30468	7.53886E-5	-4.68085E-4
0.33675	1.30912E-4	-3.19149E-4
0.37149	2.14145E-4	-1.70213E-4
0.40624	2.97352E-4	0
0.43563	3.71355E-4	1.48936E-4
0.47305	4.73078E-4	3.82979E-4
0.51849	5.74746E-4	6.17021E-4

Table 4.5: I-V values of Yombotumtum dye (Yd) based DSSC

Voltage (V)	Current (A)	Current (A)
	Yd_under the light	Yd_in the dark
6.89655E-4	-0.01541	-1.09933E-4
0.01448	-0.01541	-7.02139E-5
0.03931	-0.01507	-1.42773E-4
0.06069	-0.01459	-5.81728E-5
0.08069	-0.01426	-1.41053E-4

0.10276	-0.01358	-1.10716E-4
0.12414	-0.0129	-1.32296E-4
0.14483	-0.01215	-9.44522E-5
0.16621	-0.01154	-1.09933E-4
0.18621	-0.01066	-6.69294E-5
0.20966	-0.00998	3.03373E-5
0.23034	-0.00917	2.33785E-4
0.24966	-0.00828	2.77258E-4
0.26759	-0.00747	4.32541E-4
0.28759	-0.00652	5.88889E-4
0.30828	-0.00543	8E-4
0.32621	-0.00435	0.00107
0.34483	-0.00299	0.00133
0.36138	-0.0015	0.00159
0.37586	-2.09734E-4	0.0017
0.39103	0.00169	0.00197
0.40552	0.00366	0.00229
0.41517	0.00556	0.00261
0.42483	0.00773	0.00299
0.43724	0.01072	0.00332
0.44483	0.01234	0.00332

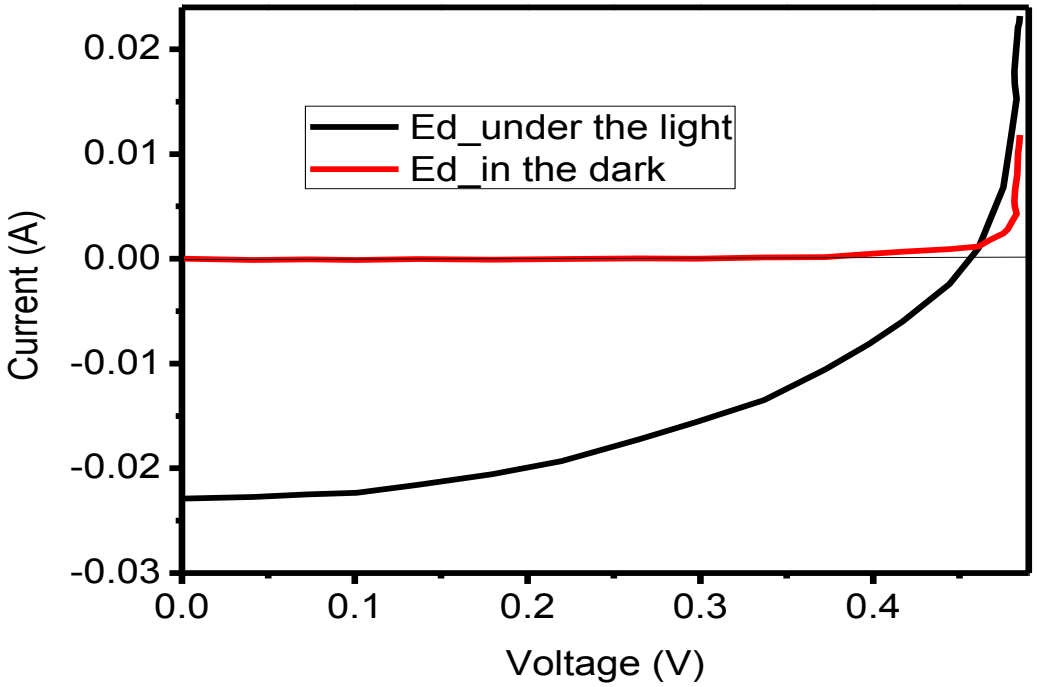

Figure 4.16: Dark and illuminated I-V curves from the fabricated Eosin-Y DSSC

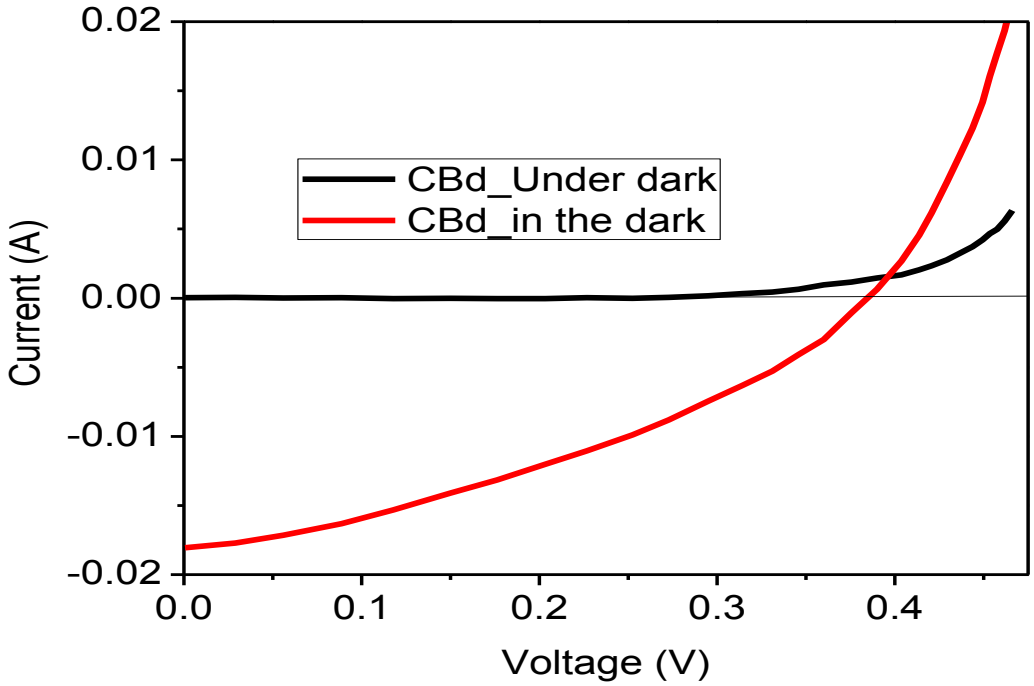

Figure 4.17: I-V curve of black cherry DSSC based on biosynthesized ZnO (Z_2)

Table 4.6: I-V values of Eosin-Y(Ed) DSSC and black cherry (CBd) DSSC based on biosynthesized ZnO (Z_2)

Voltage (V)	Current (A)	Current (A)	Voltage (V)	Current (A)	Current (A)
	Ed_Under the light	Ed_in the dark		CBd_in the dark	CBd_Under the Light
0.00121	-0.0229	0	7.24138E-4	3.14936E-5	-0.01805
0.04152	-0.02273	-1.16856E-4	0.02897	5.36093E-5	-0.01772
0.07257	-0.0225	-4.80197E-5	0.05586	5.56656E-6	-0.01716
0.10113	-0.02232	-1.00771E-4	0.0886	2.43724E-5	-0.01632
0.13677	-0.02158	-2.83861E-5	0.1178	-2.36703E-5	-0.01532
0.17933	-0.02058	-8.11367E-5	0.14995	-4.31281E-6	-0.01409
0.21954	-0.01932	-3.33536E-5	0.17624	-2.30686E-5	-0.01314
0.26448	-0.01723	3.59557E-5	0.20331	-3.68595E-5	-0.01202
0.29743	-0.01561	1.70316E-5	0.22672	4.16237E-5	-0.01106
0.33682	-0.01348	1.26318E-4	0.25236	-3.10924E-6	-0.00988
0.37226	-0.01055	1.68424E-4	0.27292	5.10517E-5	-0.0088
0.39754	-0.00816	4.51575E-4	0.29501	1.69303E-4	-0.00744
0.41715	-0.00597	6.77778E-4	0.31414	3.17944E-4	-0.00631
0.44422	-0.00241	9.27778E-4	0.33108	4.37299E-4	-0.00529
0.4607	9.7931E-4	0.00116	0.3459	6.55556E-4	-0.00409
0.46758	0.00374	0.00182	0.35997	9.66667E-4	-0.00299
0.47523	0.00681	0.00243	0.37576	0.00116	-0.00106
0.47777	0.00953	0.0028	0.39003	0.00147	6.42438E-4
0.48034	0.01232	0.00358	0.40368	0.00169	0.00268
0.48299	0.01528	0.00427	0.41368	0.00204	0.00457
0.48181	0.0167	0.00503	0.4207	0.00235	0.00617
0.48174	0.01787	0.00554	0.42937	0.00276	0.00839

0.48219	0.0188	0.00658	0.4365	0.00324	0.01033
0.48279	0.02005	0.00732	0.44363	0.00372	0.01229
0.48338	0.0213	0.00809	0.4493	0.00423	0.01417
0.48361	0.02177	0.00914	0.45353	0.00468	0.01606
0.48379	0.02215	0.01007	0.45769	0.00499	0.01774

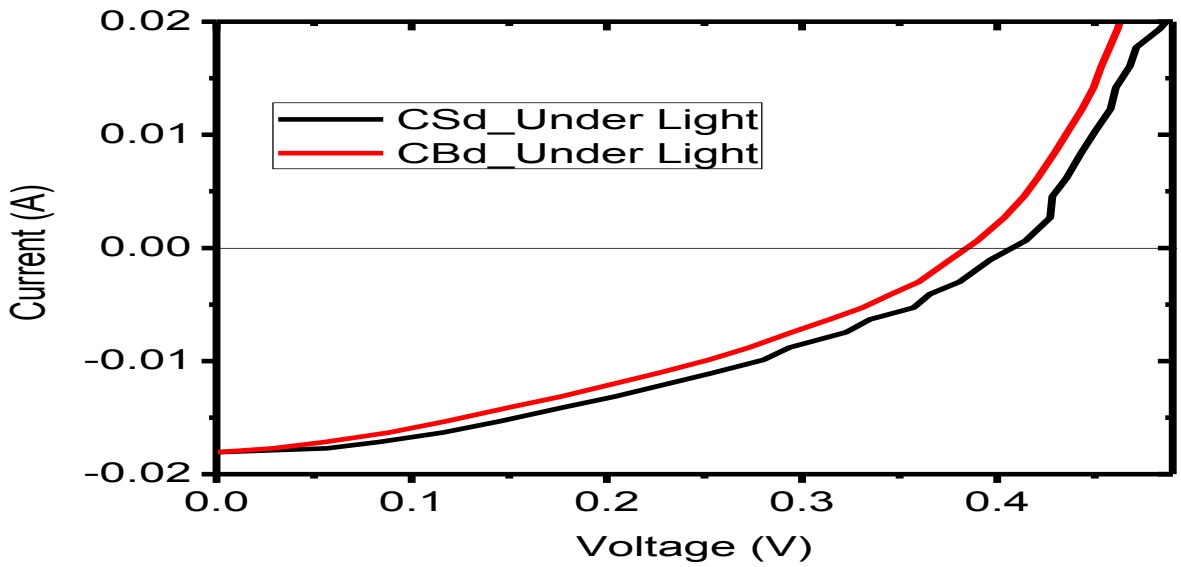

Figure 4.18: Compared I-V curve of black cherry DSSC based on Z_1 and Z_2

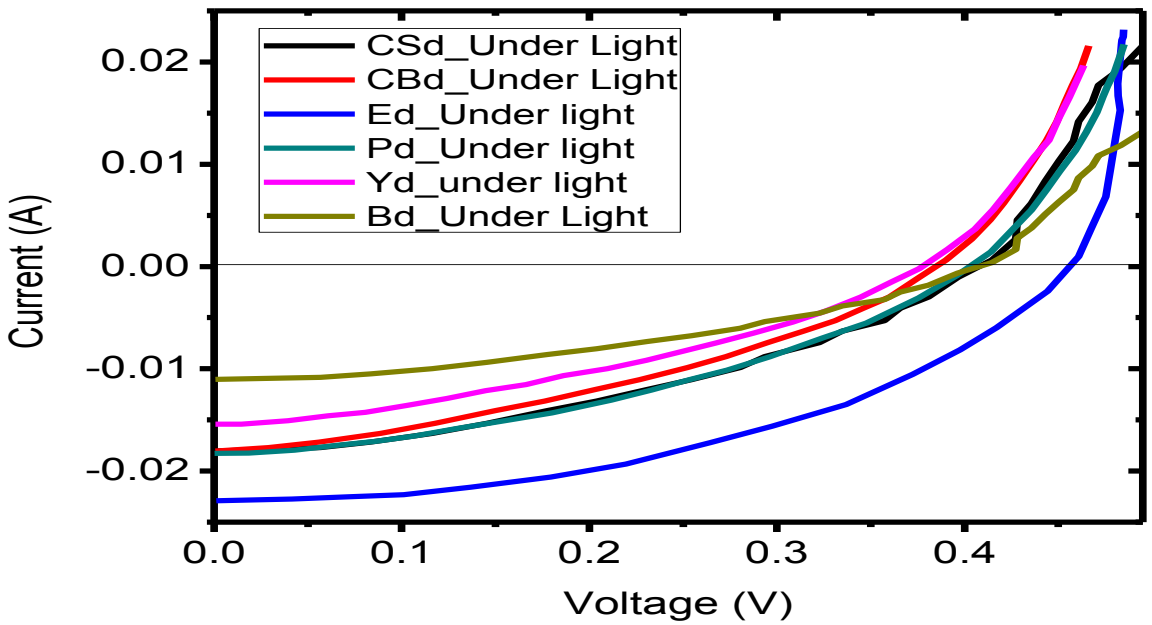

Figure 4.19: I-V curves of all the dyes based solar cell

Table 4.7: I-V values of CSd and CBd based DSSCs

Voltage (V)	Current (A)	Current (A)	Voltage (V)	Current (A)	Current (A)
	CSd_in the dark	CSd_under the Light		CBd_in the dark	CBd_Under the Light
7.24138E-4	3.14936E-5	-0.01805	7.24138E-4	3.14936E-5	-0.01805
0.05656	5.36093E-5	-0.01772	0.02897	5.36093E-5	-0.01772
0.08344	5.56656E-6	-0.01716	0.05586	5.56656E-6	-0.01716
0.11619	2.43724E-5	-0.01632	0.0886	2.43724E-5	-0.01632
0.14539	-2.36703E-5	-0.01532	0.1178	-2.36703E-5	-0.01532
0.17754	-4.31281E-6	-0.01409	0.14995	-4.31281E-6	-0.01409
0.20383	-2.30686E-5	-0.01314	0.17624	-2.30686E-5	-0.01314
0.2309	-3.68595E-5	-0.01202	0.20331	-3.68595E-5	-0.01202
0.2543	4.16237E-5	-0.01106	0.22672	4.16237E-5	-0.01106
0.28041	-3.10924E-6	-0.00988	0.25236	-3.10924E-6	-0.00988
0.29361	5.10517E-5	-0.0088	0.27292	5.10517E-5	-0.0088

0.32259	1.69303E-4	-0.00744	0.29501	1.69303E-4	-0.00744
0.33486	3.17944E-4	-0.00631	0.31414	3.17944E-4	-0.00631
0.35725	4.37299E-4	-0.00529	0.33108	4.37299E-4	-0.00529
0.36563	6.55556E-4	-0.00409	0.3459	6.55556E-4	-0.00409
0.38083	9.66667E-4	-0.00299	0.35997	9.66667E-4	-0.00299
0.39645	0.00116	-0.00106	0.37576	0.00116	-0.00106
0.41466	0.00147	6.42438E-4	0.39003	0.00147	6.42438E-4
0.42726	0.00169	0.00268	0.40368	0.00169	0.00268
0.42826	0.00204	0.00457	0.41368	0.00204	0.00457
0.43559	0.00235	0.00617	0.4207	0.00235	0.00617
0.44317	0.00276	0.00839	0.42937	0.00276	0.00839
0.4503	0.00324	0.01033	0.4365	0.00324	0.01033
0.45816	0.00372	0.01229	0.44363	0.00372	0.01229
0.46079	0.00423	0.01417	0.4493	0.00423	0.01417
0.46801	0.00468	0.01606	0.45353	0.00468	0.01606
0.47148	0.00499	0.01774	0.45769	0.00499	0.01774

Table 4.9: I-V values from the fabricated cells based on commercial ZnO (Z_1)

Dye	V_{oc} (V)	I_{sc} (mA)	P_{max} (mW)	FF	Ŋ (%)
Beetroot (B_d)	0.4147	11.03	1.72	0.3758	0.430
Yombotumtum(Y_d)	0.3910	15.41	2.11	0.3502	0.528
Pawpaw leaf (P_d)	0.4140	18.28	2.72	0.3594	0.68
Black Cherry (CS_d)	0.4147	18.05	2.811	0.3757	0.703
Eosin-Y (E_d)	0.4607	22.90	4.642	0.4400	1.161

Table 4.10: I-V values from the fabricated black cherry cell based on biosynthesized ZnO (Z_2)

Dye	V_{oc} (V)	I_{sc} (mA)	P_{max}(mW)	FF	η (%)
Black Cherry (CB_d)	0.3900	18.05	25.06	0.3560	0.63

CHAPTER FIVE

5.0 Conclusion and Recommendation

5.1 Conclusion

Five dyes were used as photo sensitizers for the fabrication of ZnO based DSSCs, which include natural dyes from pawpaw leaf, black cherry and beetroot, mineral dye from Yombo tumtum and synthetic dye from Eosin-Y. Black Cherry has average absorption of 1.7184 with energy band gap of 1.79 eV. The absorption spectra obtained from these biological and mineral dyes, which is high within the visible region, are in favor of the devices fabricated. Thus, the black cherry, which showed higher absorbance than other natural dyes, has higher conversion efficiency when compared to other natural dyes used.

The photoelectric performance of the cells based on these dyes showed that the efficiency of pawpaw leaf is 0.68%, beetroot is 0.43%, black cherry is 0.7% and Yombo tumtum is 0.53%. Z_1 based solar cell fabricated from Eosin-Y has highest performance of 1.161 %. Among natural and mineral dyes, solar cell fabricated from Black Cherry exhibits highest efficiency of 0.708 %. Solar cell based on Z_2 fabricated using optimized dye (Black Cherry) as an active material fabricated and compared with Z_1. Both cells have the same I_{sc} of 18.05 mA but different V_{oc} as in figure 4.18, of 0.4147 and 0.3900 V for Z_1 and Z_2, respectively. The black cherry based on biosynthesized ZnO has power conversion efficiency of 0.63%.

Biosynthesized ZnO nanoparticle from bitter leaf is promising as buffer layer in solar cells as it transmits nearly all the visible light to the active material. Natural dyes as sensitizers for DSSCs are promising alternative to the synthetic and inorganic solar cells due to its simple preparation technique, environment friendliness, wide availability and low-cost when compared with conventional cells.

5.2 Recommendation for Further Study

The major challenge in the fabrication and commercialization of DSSCs are the low conversion efficiency and stability of the cell. The degradation of the cell based on dye sensitization, undesirable electrolyte properties and poor contact with the electrodes are the main causes of the poor performance of DSSCs. To enhance the performance of the DSSCs, several research directions suggested improving the:

(i) Dye stability by finding the optimum parameters to slow dye degradation;

(ii) Dye structure to absorb more light at longer wavelengths of 780-2500 nm (the near-infrared region, NIR).

(iii) Mechanical contacts between the layers in DSSCs. Thus, the choice of materials is very important in the fabrication and deployment of DSSCs because the conversion efficiency and stability of the cell do not depend on a single factor alone.

REFERENCES

Arjunan, T.V.; Senthil, T.S. (2013), Review Dye-Sensitized Solar Cells. *Mater. Tech*., 28, 9-14.

Bagher, A.M. (2016), Introduction to natural Dye-Sensitized Solar Cells. *Eng. Phys*., 1(1) 1-7.

Bahramian, A. (2013), Efficiency of Dye-Sensitized Solar Cells Based on Coral-like TiO2 Nanostructured Films: Synthesis and Physical Characterization, *Ind. Eng. Chem. Res*. 52 (42), pp 14837–14846.

Bailey, M.; Park, J.; Dhirani, A. (2002), Natural dye-sensitized solar cell. Department of chemistry, University of Toronto. http://www.chem.utoronto.ca/staff/DHIRANI/solar%20cell.pdf

Bisquert .J.; Cahen, D.; Hodes, G.; Rühle, S.; Zaban, A., (2004), Physical, chemical principle of PV conversion with nanoparticle mesoporous DSSCs. *J. Phys. Chem. B*, 108, 8106-8118.

Carlson, D.; Wronski, C. (1985), Topics in Applied Physics: Amorphous semiconductor: Amorphous silicon solar cells.

Chandiran, A. K. (2014), Analysis of Electron Transfer properties of ZnO and TiO_2 photoanodes for Dye-Sensitized Solar Cells. *ACS Nano*, 8(3), 2261-2268.

Chang, H.; Kao, M.J.; Huang, K. D.; Hsieh, T. J.;, Chien, S. H. (2010), Application of TiO_2 nanoparticles coated multi-wall carbon nanotube to Dye-sensitized Solar Cells. *J. Nanoscience and Nanotchnol*, 10, 7671-7675.

Chergui, Y.; Nehaoua, N.; Mekki, D.E. (2011), Comparative Study of Dye-Sensitized Solar Cell Based on ZnO and TiO2 Nanostructures, Solar Cells - Dye-Sensitized Devices, Prof. Leonid A. Kosyachenko (Ed.), ISBN: 978-953-307-735-2,InTech,Availablefrom: http://www.intechopen.com/books/solar-cells-dye-sensitizeddevices/comparative-study-of-dye-sensitized-solar-cell-based-on-zno-and-tio2-nanostructures

Chiba, Y.; Islam, A.; Watanabe, Y.; Komiya, R.; Koide, N.; Han, I. (2006), Dye-Sensitized Solar Cells with Conversion Efficiency of 11.1%, *Jpn .J. Appl. Phy*., 45(25), 638-640.

Culity, B. D. (1987). Elements of X-ray diffraction 2nd ed., Addison-Wesley, USA

Dai, Q.; Raban, J. (2002), Inorganic chem., 26 (4), 421-426.

Dixit, A.; Dixit, S.D.; Rai, A.; Dwiveck, C.K. (2017), Dye-Sensitized Solar Cells-A review. *Int. J. Emerg. Tech. Adv. Eng*., 1(1), 154-161.

En.wikipedia.org.

Ferber, J.; Stangl, R.; Luther, J. (1998), *Sol. Energy Mater. Sol. Cells*, 53, 29.

Furukawa, S.; Lino, H.; Iwamoto, T.; Kukita, K.; Yamauchi, S. (2009), Characteristics of Dye-Sensitized Solar Cell using natural Dye. *Thin Solid film*, 519, 526-529.

Gao .Y et al., (2012), Journal of Photochemistry and Photobiology A: chemistry, 245, 66-71.

Gratzel, M. (2001), Molecular photovoltaic that mimic photosynthesis. *Pure Appl. Chem* 73(3), 459–467.

Gratzel, M. (2003), Review Dye-sensitized Solar Cells. *J. Photochem. Photobio*., 4, 145-153.

Green, A.N.M.; Chandler, R.E.; Haque, S. A; Nelson, J.; Durrant, J. R. (2005), Transient absorption studies and numerical modeling of Iodine photoreduction by nanocrystalline TiO_2 films. *J. Phys. Chem. B*, 109, 1, 142-150.

Gregg .B.A. et al., (2001), J. Phys. Chem B., 105, 1422-1429.

Greijer, A. H.; Hagfeld, A. (2003), Degradation mechanisms in a dye-sensitized solar cells studied by UV-VIS and IR spectroscopy. *Sol. Energy*, 75, 169-180.

Hagberg et al., (2008), Molecular Engineering of organic sensitizers for Dye-Sensitized solar Cells Applications. *J. Am. Chem. Soc.*, 130, 6259-6266.

Hagfeidt .A. and Gratzel .M, (2000), Acc,Chem.Res. 33, 269.

Harish Kumar, H. and Rani, R.(2013). Structural and Optical Characterization of ZnO Nanoparticles Synthesized by Microemulsion Route. *Int. Lett. Chem., Phy. and Astro.* 14, 26-36.

Hinsch , A.; Kroom, J. M.; Kern, R.; Uhlendorf, I.; Holzock, J.; Meyer, A.; Ferber, J. (2001), Long-term stability of dye-sensitized solar cell. *Prog. Photovolt. Res. Appl.* 9, 425-438.

http:/www.keithley.com/solar_cell.

Hug, H.; Bader, M.; Mair, P.; Glatzel .T. (2014), Biophotovoltaics: Natural pigments in dye-sensitized solar cells. *Appl. Energ.*, 115, 216-225.

Huo .J. Hu, Y.; Jiang, H.; Huang, W.; Li, Y.; Shao, W.; Li, C. (2013), Mixed Solvents Assisted Flame Spray Pyrolysis Synthesis of TiO_2 Hierarchically Porous Hollow Spheres for Dye-Sensitized Solar Cells *Ind. Eng. Chem. Res., 52* (32), 11029–11035. DO**I:** 10.1021/ie4006222

Ito, S.; Ha, N. L. C.; Rothenberger, G.; Liska, P.; Comte, P.; Zakeeruddin, S.M. (2006), Highefficiency (7.2%) flexible dye-sensitized solar cells with Ti-metal substrate for nano crystallineTiO_2 photoanode. *Chem. Comun. (camb)*, 38, 4004-4006. DOI:10.1039/b608279c

Jasim, K. E. (2011), Dye-Sensitized Solar Cells – Working principles, challenges and opportunities. IntechOpen, DOI: 10.5772/19749. Available from: https://www.intechopen.com/books/solar-cells-dye-sensitized-devices/dye-sensitized-solar-cells-working-principles-challenges-and-opportunities.

Jiang, P.; McFarland, M. J. (2004), Large scale fabrication of wafer-size colloidal crystals, macroporous polymers and nano-composites by spin coating. *J. Am. C hem. Soc*., 126(42), 13778-13786.

Jun Hyuk Yang et al., (2014), Characteristics of the Dye- sensitized solar Cells using TiO_2 nanotubes treated with $TiCl_4$. *Materials*, 7, 3522-3532.

Kato, N.; Takeda, Y.; Higuchi, K.; Takeichi, A.; Sudo, E.; Tanaka, H.; Motohiro, T.; Sano, T.; Toyoda, T. (2009), Degradation analysis of Dye-Sensitized Solar Cell module after long term stability test under outdoor working condition. *Sol. Energy mater. Sol. Cells*, 93, 893-897.

Kim, S.; Nah, Y.; Noh, Y.; Jo, J.; Kim, D. (2001), Electro deposited Pt for cost-efficient and flexible dye-sensitized solar cells. *Electrochem. Acta*, 51, 3814-3819.

Klar,S. H. L. (2005), Plant extract sensitized nanoporous Titanium Dioxide thin film photoelectrochemical cells. PhD thesis, Department of Engineering Science, Uppsala University.

Lewis, N.S. (2007), Toward cost-effective solar energy use. *Science*, 315, 798-801.

Liko, D.V.; Stergiopoulos .T.; Falaras, P.; Harikisun, R.; Desilvestro, J.; Tulloch, G. (2009), Prolonged light and thermal stress effects on industrial dye-sensitized solar cells. A micro-Raman investigation on the long-term stability of aged cells. *J. Phys. Chem. C*, 113, 9412-9422.

Lin, C.; Tsai, F.Y.; Lee, M. H.; Lee, C. H.; Tien, T. C.; Wang, L. P.; Tsai, S.Y. (2009), Enhanced performance of dye-sensitized solar cell by an Al_2O_3 charge-recombination barrier formed by low-temperature atomic layer deposition. *J. Mater. Chem*. 19, 2999-3003.

Lin, J.Y. (2012), Absorption Spectra Analysis of Natural Dyes for Application in Dye-Sensitized Solar Cells. The 31st National conference on theoretical and applied mechanics.

Mamidi, T.; Mandha, S. B.; Mishra, A. (2012), Study and Analysis of Dye-Sensitized solar Cells. *Int. J. Mod. Eng. Res*., 2 (5), 3597-3601.

Mattews, D.; Infelta, P.; Gratzel, M. (1996), Calculation of the photocurrent-potential characteristics for regenerative electrodes. *Sol. Energy matter. Sol. Cells.* 44, 119-155.

Mehmood, U.; Rahman, S.U.; Harrabi, K.; Husseini, I. A.; Reddy, B.V.S. (2015), Recent Advances in Dye Sensitized Solar Cells, *Adv. Mater. Sci. and Eng*., (2015), 1-12. http://dx.doi.org/10.1155/2014/974782

Meyer-Arendt, J.R. (1995), Introduction to classical and modern optics. 4th Ed. Prentice hall (Engle wood cliffs).

Michal Sokolsky, Martin Kusko, Michal Kaiser, Julius Cirak, (2011), Fabrication and characterization of Dye-sensitized solar cells based on Natural organic dyes. Research gate, vol. 4, (20), 26-29.

Mir, N.; Lee, K.; Paramasivam, I.; Schmuki, P. (2012), Optimizing TiO_2 Nanotube Top Geometry for Use in Dye-Sensitized Solar Cells, *Chem. Eur. J*., 18(38), 11862-11866.

Mohammed, A.A.; Ahmad A. S. S.; Azeez, W. A. (2015), Fabrication of Dye-Sensitized Solar Cells based on Titanium dioxide (TiO_2). *Adv. Mater. Phys. and Chem.*, 5, 361-367.

Narayan, M. R.; (2012), Review Dye sensitized solar cells based on natural photosensitizers. *Renew. Sust. Energ. Rev*., 16, 208-215.

Neil R. (2006), Optimizing dyes for Dye-Sensitized Solar Cells. *Angew Chem. Int. Ed Engl.*, 45(15), 2338-2345.

Noel, N.K.; Stranks, S.D.; Abate, A.; Wehrenfennig, C.; Guarnera, S.; Haghighirad, A. A.; Sadhanala, A.; Eperon, G. E.; Pathak, S. K.; Johnston, M. B.; Petrozza, A.; Herz, L. M.; Snaith, H. J. (2014), Lead - free organic – inorganic tin halide perovskite for photovoltaic applications, *Energy and Environ. Sci.* **7**(9), 3061 - 3068.

O'Regan and Gratzel, M. (1991), A low-cost, high-efficient Solar Cell based on Dye-sensitized colloidal TiO_2 films. *Nature*, 353, 737-740.

Oviri, O. K. and Ekpunobi, A.J. (2012), Fabrication and characterization of Dye-Sensitized Solar Cells using Anarcardium occidentale Sensitizer. *Pelagia research library*, 3, 3390-3395.

Pentland W. (2010), solar powered tablets to target rural students. Forbes.com LLC,

Petrovic, M.; Chellappan, V.; Ramakrishna, S. (2015), Perovskites: solar cells & Engineering applications-materials and device development. *Sol. Energy.*, 122, 678-699.

Pichot, F. and Gregg .B.A, (2000), The Photovoltage-Determining Mechanism in Dye-Sensitized Solar Cells, *J. Phys. Chem. B.* 104(1), 6 -10

Pradhan, B.; Batabyal, S. K.; Pal, A. J. (2007), Vertically aligned ZnO nanowire arrays in rose Bengal-based dye-sensitized solar cell. *Sol. Energ. Mater. Sol. Cells*, 91, 769-773.

Reshak, A. H.; Shahimin, M. M.; Shaar, S.; John, N.(2013), Surface modification via wet chemical etching of single-crystalline silicon for photovoltaic application, *Prog. Biophys. Mol. Bio*., 113(2), 327-332.

Saito, Y.; Kitamura, T.; Wada, Y.; Yanagida, S. (2002), Application of poly (3,4-ethylenedioxythiophene) to counter electrode in Dye-sensitized solar cells. *Chem. lett*, 31(10), 1060-1061.

Sharma, P. D. (2009), On keeping the world environment safer and greener.

Sima, C.; Grigoriu, C.; Antohe, S. (2010), Comparison of the dye-sensitized solar cells performances based on transparent conductive ITO and FTO, *Thin Solid Films*, 519(2), 595-597.

Singh, P. and Ravindra, N. M. (2011). Analysis of series and shunt resistance in silicon solar cells using single and double exponential models, *EMR*, 1(1), 33 -38.

Son, H. J.; Prasittichai, C.; Mondloch, J.E.; Luo, L.; Wu, J.; Kim, D.W.; Farha, O.K.; Hupp, J.T. (2013), Dye stabilization and enhanced photoelectrode wettability in water-based dye-sensitized solar cells through post-assembly atomic layer deposition of TiO_2. *J. Am. Chem. Soc*., 135, 11529–11532.

Stathatos, E (2011). Dye Sensitized Solar Cells as an Alternative Approach to the Conventional Photovoltaic Technology Based on Silicon - Recent Developments in the Field and Large Scale Applications, Solar Cells - Dye-Sensitized Devices, Prof. Leonid A. Kosyachenko (Ed.), ISBN: 978-953-307-735-2, *InTech*, Available from: http://www.intechopen.com/books/solar-cells-dye-sensitized-devices/dye-sensitized-solar-cells-as-analternative-approach-to-the-conventional-photovoltaic-technology-ba

Suhaimi, S.; Shahimin, M. M.; Alahmed, Z.A.; Chysky, J.; Reshak, A.H. (2015), Short review Materials for enhanced Dye-Sensitized solar Cell performance: Electrochemical application. *Int. J. Electrochem. Sc.*, 10, 2859-2871.

Toivola, M.; Halme, J.; Miettunen, K.; Aitola, K.; Lund P.D. (2009). Nanostructured dye-sensitized solar cells on flexible substrates-review. *Int. J. Energy Res*. 33, 1145-1160.

Veerappan, G.; Bojan, K.; Rhee, S.W. (2012), Amorphous carbon as a flexible counter electrode for low cost and efficient Dye-sensitized solar cells. *Renew. Energy*, 41, 383-388.

Wayne .P.A., (1994), Natural dyes. *J. American Bot. council*, vol 32-30.

Weerasinghe, H. C.; Sirimanne, P. M.; Simon, G. P.; Cheng, Y-B. (2011), Cold Isostatic pressing technique for producing highly efficient flexible Dye-Sensitized Solar Cells on plastic substrates, *Prog. Photovoltaic Res. Appl*., 20, 321-332.

Wenham, S.R.; Green, M.A.; Watt, M.E.; Corkish, R. (2006), *Applied photovoltaics*. 2nd Ed.[Sydney] : UNSW. Centre for Photovoltaic Engineering.

Wongchareea, K.; Meeyooa, V. and Chavadej S. (2007), Dye- Sensitized Solar Cell using natural dyes extracted from rosella and blue pea flowers, *Solar Energy materials & Solar Cells*, 91, 566-571.

Wu, J.; Lan, Z.; Hao, S.; Li, P.; Lin, J.; Huang, M.; Fang, L. and Huang, Y. (2008). Progress on the electrolytes for Dye-sensitized solar cells. *Pure Appl. Chem*. 80, 2241-2258.

www.wikimedia.com

Ye, M.; Wen, X.; Wang, M.; Locozzia, J.; Zhang, N. Lin, C.; Lin, Z. (2014), Recent advances in Dye-Sensitized Solar Cells: from photoanodes, sensitizers and electrolytes to counter electrodes. *Material Today*, 18(3), 155-162.

Yella, A.; Lee, .H. W.; Tsao, H. N.; Yi, C.; Chandiran, A. K.; Nazeeruddin, M. K.; Diau, E.W.G.; Yeh, C.Y.; Zakeeruddin, S. M.; Gratzel, M. (2011), Porphyrin-sensitized solar cells with Cobalt (11/111)-based redox electrolyte exceed 12 percent efficiency. *Science*, 334, 629-634.

Zulkifili, A. N. B.; Kento, T.; Daiki, M.; Fujiki, A. (2015), The basic research on the dye-sensitized solar cells. *J. Clean Energ. Tech*., 3(5). 382 - 387.